

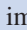


Biomechanics of Bone

10

Jacqueline H. Cole and
Marjolein C. H. van der Meulen

Key Points

- The ability of the skeleton to bear loads without fracture depends on both the applied loading conditions and the structural properties of bone.
- Many factors can alter the structural properties of bone, including aging, trauma, and disease, as well as an individual's loading history and mechanobiological response.
- Combined  imaging-modeling approaches that include contributions of bone mass, architecture, and material properties can help elucidate mechanisms of skeletal fragility.
- More realistic material mapping and mimicking of in vivo loading conditions are needed to calculate bone strength more accurately and predict fracture risk reliably for individuals.

Bone Strength and Fracture

The skeletal system has important metabolic, physiologic, and mechanical functions, including storing minerals, protecting vital organs, and bearing functional loads. Individuals constantly impose dynamic mechanical stimuli on their bones during daily activities. A healthy skeleton generally has sufficient bone strength to support these loads without fracture, but trauma, aging, and disease can compromise its structural function. With trauma, loading may exceed the load-bearing capacity of the skeleton, either healthy or otherwise, and produce fracture. Aging and many skeletal diseases reduce bone strength, thereby producing skeletal failure even under normal or non-traumatic loading conditions. Fractures result not only in individual morbidity and mortality but also in high healthcare and societal costs [1–3]. Therefore, an understanding of the factors that contribute to bone strength is critical for the prevention and treatment of skeletal fractures.

Failure of any load-bearing structure can stem from a single traumatic overload or from the accumulation of damage with repetitive loading. Here we will focus on the former: what determines whether a given load applied to a bone will result in fracture? The interaction between applied loading and the ability of a bone to bear the applied loads can be summarized in a term called *factor of risk* [4]. The factor of risk is the ratio between the load applied to a bone and the load required to

J. H. Cole (✉)
Joint Department of Biomedical Engineering,
University of North Carolina–Chapel Hill and North
Carolina State University, Raleigh, NC, USA
e-mail: jacquecole@ncsu.edu

M. C. H. van der Meulen
Schools of Biomedical Engineering and Mechanical
& Aerospace Engineering, Cornell University,
Ithaca, NY, USA

fracture that bone, or *failure load*. If the applied load exceeds the failure load for any given bone, then the factor of risk is greater than one, and fracture will occur. To predict fracture accurately for a particular skeletal site, characteristics of both the applied and failure loads must be considered. The load applied to the bone is influenced by the type of activity or trauma, the impact location and direction, and any protection imparted by overlying soft tissues. The failure load for that bone is determined by the quantity, distribution, and structural arrangement, and characteristics of the constituent components of the bone tissue [5]. The ability of the skeleton to resist fracture under applied loading varies with aging and disease, primarily through changes in these components of failure load. Our focus here will be on the determinants of whole bone strength and factors that affect whole bone behavior when loaded.

The mechanical function of bone is strongly shaped by the *in vivo* loading experienced by the skeleton. Bone tissue is exquisitely mechanosensitive, and bone cells respond to mechanical stimuli by altering turnover to increase or decrease the amount of tissue present, which in turn alters the tissue architecture and material properties [6, 7]. Therefore, the loading history experienced throughout an individual's lifetime contributes to these bone properties and greatly impacts skeletal structure and the failure load of bone [8]. This process of mechanoregulation, whereby physical forces influence cell behavior and bone (re)modeling, is an active field of research called *mechanobiology*. This concept of functional adaptation in response to mechanical stimuli has been around since the late 1800s, pioneered by the work of Roux [9] and Wolff [10]. It has been studied extensively in many *in vivo*, *in vitro*, and *in silico* models, and more recent studies have combined these mechanobiology models with new “omics” technologies (e.g., genomics, proteomics) to probe the effects at the molecular level in an emerging area of *mechanomics* (reviewed by [11]).

Factors Contributing to Whole Bone Strength

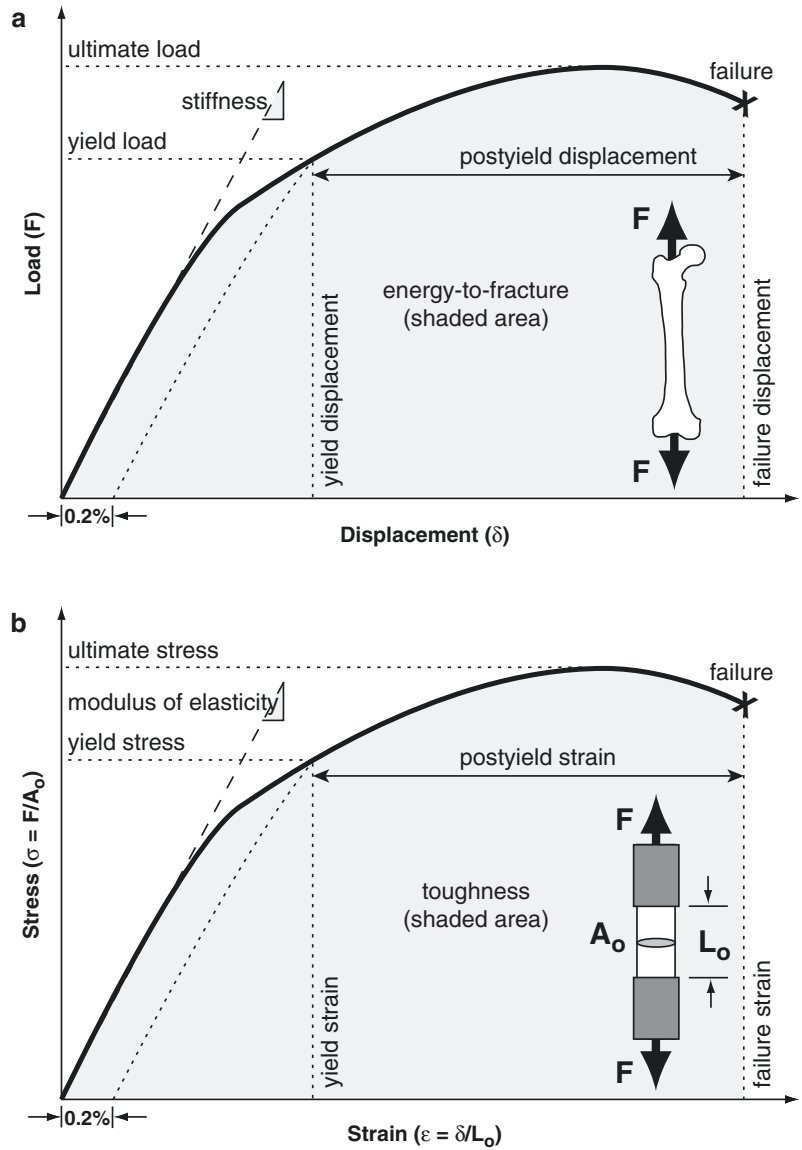
Measurements of whole bone strength and other structural properties are different for different

types of loading. *In vivo* the skeleton withstands a complex array of different types of applied loads during the course of its various activities, such as walking, stair climbing, and lifting objects [12, 13]. To characterize the mechanical behavior of a whole bone, more simple loading modes – axial (tension or compression), bending, or torsion (twisting) – are often applied during mechanical testing in the laboratory. Because bone is metabolically active and capable of dynamic adaptation in response to loading, its properties will vary over time, a factor that must be considered when comparing bone properties or making fracture predictions.

True structural properties of bone can only be measured with *ex vivo* mechanical testing, so our understanding about bone properties comes primarily from studies using whole cadaver or animal bones or bone biopsies. When a force is applied to a whole bone, the structure experiences measurable displacement, or deformation (Fig. 10.1a). When the load is examined as a function of the displacement, the resulting curve has several distinct characteristics: an initial linear or *elastic* region, a nonlinear region with a maximum defined as the ultimate point, and a failure point at which the bone fractures and can no longer withstand the applied load. Applied loads that fall within the initial linear range can be resisted without permanently deforming the bone or causing failure.

The two most critical measures obtained from load-displacement data are structural stiffness and strength. The stiffness of a whole bone is the resistance to deformation for a given applied load and is the slope of the linear portion of the load-displacement curve. For a whole bone, the structural strength is the maximum or *ultimate* load that the bone can withstand. Whole bone stiffness and strength will have different values for different loading modes, such as compression, bending, and torsion, and these values depend on the intrinsic properties of the bone tissue, how much tissue is present, and the geometric arrangement of the tissue. For example, the failure strength of a vertebral body will be different when loaded in compression than in bending. Stiffness and strength are distinct parameters but are often correlated. Other parameters of interest include the yield point (the transi-

Fig. 10.1 (a) Load-displacement behavior for a structural test such as a whole bone. The structural stiffness is determined from the initial linear region. Yield is the transition point from linear to nonlinear behavior. Structural strength is the load required to fail the whole bone. Energy-to-fracture is the area under the entire curve (shaded). (b) Stress-strain behavior for a tissue materials test. These measurements are independent of specimen size and shape. The modulus of elasticity, or tissue stiffness, is determined from the initial linear region; tissue strength is the maximum or ultimate stress; and toughness is the shaded area. Both structural and material parameters depend on loading mode (tension, compression, bending, or torsion)



tion between the linear and nonlinear regions), post-yield displacement (the amount of deformation between the yield and failure points), and energy-to-fracture or work-to-fracture (the area under the entire load-displacement curve), which represents the amount of energy the bone dissipates up until failure or, equivalently, the amount of work the applied load performs to deform and break the bone.

Structural properties, such as whole bone stiffness and strength, are *extrinsic properties* that vary with the size and shape of the bone being tested. The forces and deformations of the whole

bone also create internal forces and deformations within the bone tissue that are known as stresses and strains. Material characteristics, such as stresses and strains, are *intrinsic properties* that are independent of bone size and shape. These material properties can be measured on small, homogeneous tissue samples, such as a machined microbeam. Similar to a whole bone test, a bone materials test examines deformation in response to an applied load, and the resulting stress-strain curve can be examined for properties analogous to the ones for a whole bone test (Fig. 10.1b), such as modulus of elasticity (tissue stiffness), ultimate

stress (tissue strength), post-yield strain, and toughness (energy dissipated per unit of tissue up until failure). Similar to structural properties, material properties depend on the direction or mode of loading. More details about bone material properties will be discussed in a later section.

Whole bone behavior depends on the behavior of the constituent tissues, cortical and cancellous bone. During whole bone bending, for example, the behavior is dominated by cortical bone geometry and material properties in the diaphysis. Cortical and cancellous bone are both complex structures, and their behavior depends on similar factors as those for whole bone strength, as discussed below. The continuum properties of these bulk tissues are referred to as *apparent* properties, which is at a length scale below the whole bone properties but above the tissue material properties. These properties can be determined using mechanical tests on specimens in this range, such as a cancellous bone core from a vertebra. The porous structure of cancellous bone and its location in vertebral bodies and in the ends of long bones are important for distributing joint contact forces during daily activities, but they also make the tissue more susceptible to the surface-focused resorption that occurs with aging and skeletal disease. The structural behavior of cortical and cancellous bone is governed chiefly by the quantity of bone tissue present (bone mass or density), the size and spatial arrangement of that tissue (cortical geometry and cancellous architecture), and the intrinsic tissue material properties [14–18]. Alterations in any of these components could compromise the integrity of the overall bone structure and its ability to bear loads. Although most *in vivo* imaging tools measure bone mass or apparent bone mineral density (apparent BMD), these measures alone do not fully explain variations in mechanical properties observed experimentally. In the following sections, the contribution of bone mass, architecture, and material properties to the structural behavior of cancellous bone will be described, as well as the clinical and laboratory tools used to characterize them. The role of bone quantity (bone mass or density) has been studied most extensively, although the effects of architecture and tissue

material properties have been examined more in recent years through technological advancements in imaging and image-based computer models.

Bone Quantity

The most-studied determinant of bone structural behavior is the overall quantity of bone at a given skeletal site. Bone mass and bone mineral density (BMD) are most commonly assessed *in vivo* using dual-energy X-ray absorptiometry (DXA, see Chap. 7), which evaluates the inorganic mineral phase of bone with minimal radiation exposure to patients. DXA scans can be performed for large regions, such as the lumbar spine, proximal femur, forearm, or even the whole body, thereby providing a noninvasive global measure of bone mass. However, DXA-based BMD alone cannot account for differences in mineral distribution and bone structure and only partially discriminates individuals who will fracture from those who will not [19, 20]. This is not surprising: DXA scans are two-dimensional and provide projected areal measurements of BMD (aBMD), which integrate geometric and material contributions into BMD values and create a size bias that overestimates the volumetric mineral density for larger individuals [21]. Because the resolution of DXA is relatively low (on the order of 1 mm), cortical bone tissue cannot be distinguished from cancellous tissue, architectural features of cancellous bone (on the order of 0.1 mm) cannot be captured, and the mineral distribution within the bone tissue cannot be measured. Because unmineralized tissues do not inherently attenuate X-rays, DXA scans cannot evaluate the organic phase of bone or the soft tissues surrounding bone. DXA aBMD correlates well with *in vitro* vertebral failure load in compression [22].

Quantitative computed tomography (QCT) is a true three-dimensional method based on X-ray imaging that overcomes many of the limitations of DXA, though with a slightly higher radiation exposure for the patient. The resolution of this technique is typically better in the scan plane (~0.5 mm) than axially between slices (~1 mm). QCT provides volumetric measures of BMD

(vBMD) and can distinguish between cortical and cancellous bone, but it cannot accurately capture cancellous architecture or mineral distribution. Due to recent advancements in clinical imaging technology, high-resolution peripheral QCT (HR-pQCT) can resolve bone features much more accurately than DXA or QCT [23], with isotropic voxel sizes of 82 μm (spatial resolution of about 130–150 μm) [24] or 61 μm in second-generation scanners. HR-pQCT also measures volumetric BMD, but it can visualize trabecular bone much better than QCT, especially in newer scanners, enabling some quantification of trabecular architecture [25]. However, it can currently only examine peripheral sites, such as the distal forearm and tibia. Because the spatial resolution is similar to the thickness of a trabecula, several of the architectural parameters cannot be directly measured (trabecular thickness and separation) but are derived from bone volume fraction (BV/TV) and trabecular number, assuming a plate model [26, 27].

For cancellous bone, quantity is typically measured either by BV/TV, which is the volume of bone tissue present within the total volume of interest, or by apparent BMD, which is the mass of bone tissue present within the total volume. Additionally, tissue mineral density, or TMD, which is the mass of bone tissue within only the volume containing bone, can be computed as the product of BV/TV and apparent BMD. Variations in bone mass can produce 100-fold differences in the cancellous bone stiffness within an individual's tibial metaphysis, ranging from 4 to 433 MPa [28].

In the laboratory, empirical formulations have been developed to predict bone tissue strength and apparent tissue stiffness from apparent BMD [14, 29–33]. These relationships are often expressed in power law form, with the exponent (b) relating apparent BMD (ρ) to cancellous stiffness or strength (S) and ranging from 1 to 3:

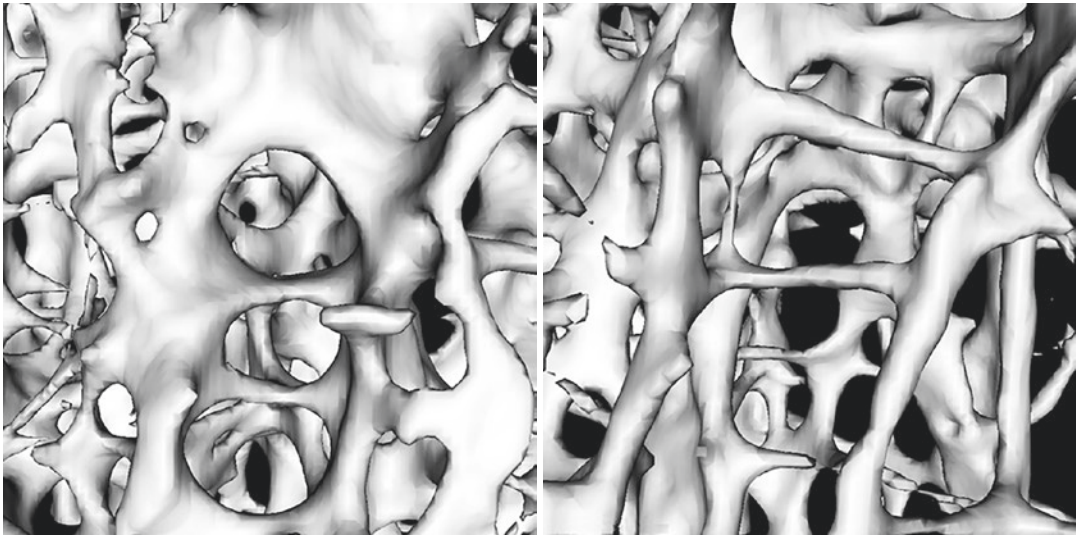
$$\rho = aS^b$$

The coefficient a is a constant that scales the ρ – S relationship and is based on experimental data in bone specimens from various anatomic sites. As a result, for a relationship with an exponent greater than 1, a decrease in apparent BMD (or

BV/TV) will result in a substantially greater decrease in stiffness and strength. For example, a 21% reduction in bone mass would predict a 38% reduction in cancellous stiffness and strength for a squared relationship and a 51% reduction for a cubic relationship (Fig. 10.2). Regardless of the relationship used, apparent BMD and BV/TV obtained experimentally or from micro-computed tomography (micro-CT) can explain 60–85% of the variability in compressive apparent stiffness and strength for human cancellous bone [34–38]. Although bone mass measurements generally have a high explanatory power for bone mechanical properties, these surrogate measures only capture one aspect of bone strength and cannot capture differences in how this mass is distributed. While mass is critical to bone integrity, additional factors are clearly needed to determine whether an individual will or will not fracture.

Several adjunct geometric parameters have been derived from DXA to try to improve fracture risk assessments beyond aBMD, including hip geometry metrics (e.g., hip structural analysis, hip axis length, neck-shaft angle) and a spine texture parameter. The only hip measure approved by the International Society for Clinical Densitometry (ISCD) for clinical hip fracture risk assessments is hip axis length (HAL), the distance through the femoral neck from the base of the greater trochanter to the inner pelvic rim [39, 40]. HAL is associated with hip fracture risk in women [39, 41, 42] and perhaps also in men [43], independent of aBMD and FRAX[®], which is a 10-year fracture probability assessment using clinical risk factors [44].

Trabecular bone score (TBS), a gray scale textural analysis of DXA lumbar spine scans, was more recently developed to provide some information about bone microstructure [45]. Since its approval by the Food and Drug Administration in 2012, TBS has been shown in several studies to predict fractures in both women and men independent of lumbar spine aBMD [46–52]. A meta-analysis of 14 international cohorts showed that TBS predicts major osteoporotic fracture in both women and men, with an overall 32% increased fracture risk per



Normal

74-year-old female
 T-score = -0.8
 BV/TV = 12.7%
 Tb.Th = 117 μm
 Modulus, $E = 844 \text{ MPa}$
 Strength, $\sigma_u = 3.5 \text{ MPa}$

Osteoporotic

92-year-old female
 T-score = -2.6
 BV/TV = 10.0% (-21% vs. Normal)
 Tb.Th = 90 μm
 Modulus, $E = 470 \text{ MPa}$ (-44%)
 Strength, $\sigma_u = 2.1 \text{ MPa}$ (-40%)

Fig. 10.2 Micro-CT images of two cancellous cores taken from the center of the L2 vertebra of two different females. Measured T-score, bone volume fraction (BV/TV), trabecular thickness (Tb.Th), and apparent modulus and strength are indicated, as well as percent differences for the osteopo-

rotic female relative to the normal female. For this 21% bone loss, a squared power law relationship would predict a 38% reduction in modulus and strength, and a cubic power law would predict a 51% reduction, both of which are comparable to the 40–44% reductions found experimentally

standard deviation decrease in TBS after adjusting for age and FRAX[®] probability [53]. Therefore, TBS seems to be a promising tool to aid in fracture risk prediction, but is only weakly correlated with aBMD at the lumbar spine ($r = 0.33$) or femoral neck ($r = 0.27$) [40]. Furthermore, in ex vivo testing of 16 human cadaver lumbar vertebrae, while TBS was significantly correlated with compressive stiffness independent of DXA aBMD, it did not significantly improve prediction of vertebral bone strength over aBMD alone [54]. While not a direct measure of bone architecture, TBS does correlate moderately with some trabecular measures based on comparisons with micro-CT in ex vivo studies and with HR-pQCT in in vivo studies, which may explain its ability to aid fracture prediction.

Bone Geometry and Architecture

For cortical bone, geometric parameters – such as the periosteal diameter, cross-sectional area, cross-sectional moment of inertia, and a geometric indicator of failure strength called the section modulus – all influence the whole bone structural behavior [55]. For bones loaded in bending, the cross-sectional moment of inertia (I) is a geometric measure of the distribution of bone about a central or *neutral* plane indicative of the bone's resistance to bending deflection, computed as follows for a hollow circular cross section [56]:

$$I = \frac{\pi}{4} (R_p^4 - R_e^4)$$

R_p is the periosteal radius, and R_e is the endosteal radius, computed about the neutral plane.

For bones loaded in torsion, the polar moment of inertia (J) is the distribution about the longitudinal or *neutral* axis and represents the bone's resistance to angular deflection or twist, computed as follows for a hollow circular cross section [56]:

$$J = \frac{\pi}{2} (R_p^4 - R_e^4) = 2I$$

The section modulus (Z) represents a whole bone's resistance to bending or torsional loads and is computed as follows for a hollow circular cross section:

$$Z_{\text{Torsion}} = \frac{J}{R_p} = \frac{\pi}{2R_p} (R_p^4 - R_e^4) = 2Z_{\text{Bending}}$$

For a long bone loaded in bending, as seen in the proximal femur, both the size and geometric distribution of cortical bone relative to the loading axis contribute to the whole bone's resistance to applied loads and thus to fracture. To illustrate this concept, we will compare the properties of three "bones" that have a circular cross section, one solid and two hollow with cortical thickness equal to 20% of the periosteal diameter (Fig. 10.3). Comparing the solid "bone" to the first hollow one, which is comparable in size with the same periosteal diameter, the hollow one has a 25% smaller cortical area but only a 6% lower section modulus, which is proportional to the bending failure strength. If we compare the same solid "bone" to another hollow "bone" that has the same cortical area as the solid "bone" yet maintains the same cortical thickness as the first hollow "bone," then the new hollow one will have a 25% larger periosteal diameter, resulting in a 70% larger section modulus (and thus bending strength). Therefore, even small changes in overall bone size can compensate for losses in bone strength when the remaining bone is redistributed farther from the neutral plane or axis. Periosteal expansion is a common compensatory adaptation in aging bone that increases bending strength to help offset other losses.

Similarly for cancellous bone, the size and spatial arrangement of trabeculae that make up the cancellous architecture also play a key role in the structural competence of bone. As early as the

mid-nineteenth century, increased fracture incidence was observed in older patients with thinning bone [57]. Two different sites of cancellous bone with similar apparent BMD can vary substantially in their stiffness and strength due to differences in tissue architecture [58, 59]. In addition, the architecture of cancellous bone often has a preferred orientation, creating substantially different modulus and strength values when bone from a given anatomic site is loaded in different directions, a characteristic called material anisotropy. In human vertebrae, for example, the primary trabecular orientation is superior–inferior, corresponding to the strongest direction when loaded [60]. Cancellous bone is nearly twice as strong when loaded along the superior–inferior direction of the spine than when loaded in the anterior–posterior or medial–lateral directions [58]. Therefore, characterizing the cancellous bone structure is important for understanding the relationship between architecture and mechanical properties.

Cancellous bone architecture cannot be directly measured with DXA, although as mentioned previously, TBS from DXA moderately correlates with some architectural parameters, in particular connectivity density, trabecular number, and trabecular separation [45, 54, 61–65]. Although QCT cannot accurately measure cancellous architecture, geometry-based metrics from QCT have been successful at predicting hip fracture [66–75] and spine fracture [71, 76, 77] in men and women, although most studies show limited or no improvement over DXA aBMD. HR-pQCT can measure both cortical and cancellous bone architecture with high reproducibility, with coefficients of variation (CV) reported at <5% for cortical thickness, BV/TV, and trabecular number, thickness, and separation [27, 78, 79]. Cortical porosity was less reproducible, with CV of 12–14% at the distal radius and 4–8% at the distal tibia, although the least significant change was <1% and deemed small enough to detect group differences and longitudinal changes [78]. HR-pQCT measures generally have good agreement with micro-CT measures in cadaver bone ($r^2 = 0.59–0.98$) [80], with stronger correlations for parameters of trabecular

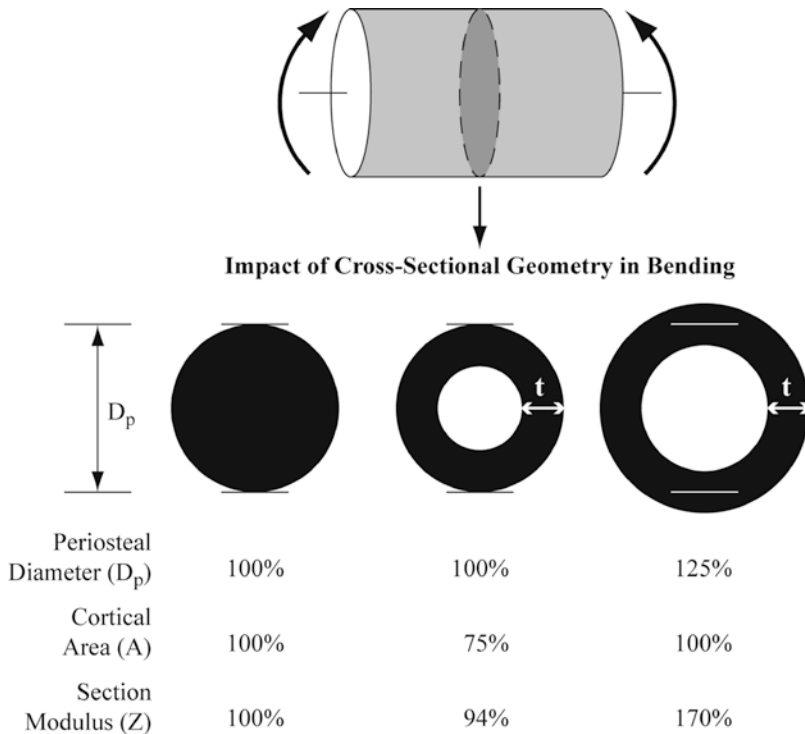


Fig. 10.3 Variations in the size and distribution of bone mass in a cortical bone cross section influence the section modulus, which is proportional to the bending failure strength of the whole bone. The resorption of bone on the endosteal surface or the apposition of bone on the periosteal surface may change the cortical thickness (t) or the distribution of bone

about the loading axis, thereby altering the ability of the bone to resist fracture. For example, compared to the reference bone (left), a bone of the same girth but with less material (middle) will be slightly weaker, but a bone with the same amount of material distributed farther away from the neutral axis of the bone (right) will be much stronger

plates compared with trabecular rods [81]. Almost all of the studies assessing fracture prediction with HR-pQCT have been retrospective cross-sectional studies. Overall, HR-pQCT measures (vBMD + architecture) can better distinguish between subjects with and without fractures than DXA (aBMD only), particularly at the forearm (reviewed by [80]). The one prospective study to date assessed fracture prediction in French postmenopausal women from the OFELY cohort and showed that vBMD and architecture (especially trabecular number and connectivity density) at both the radius and tibia predicted the risk of all types of fractures [82].

Computational anatomy approaches provide information about the spatial distribution of mass and geometric features within QCT scans [83]. Anatomical structures are modeled as curves, surfaces, or volumes and, using statistical para-

metric mapping (SPM) [84], these features are examined across multiple subjects to determine changes associated with disease progression or treatment [85–90]. Various techniques fall into this category, including voxel-based morphometry (VBM) for mapping volumetric BMD [69] and tensor-based morphometry (TBM) for mapping volume (shape and size) changes via contraction-expansion maps [70]. Additional techniques combine both density and shape mapping, such as statistical shape and density modeling (SSDM) [68, 91], and cortical bone mapping (CBM), which includes volumetric distributions of cortical BMD, endocortical trabecular BMD, and cortical thickness [74, 92]. Of these techniques, only CBM and SSDM have been compared with DXA, showing only a modest improvement in fracture prediction compared to DXA aBMD.

Similar to bone mass measures, trabecular microarchitectural parameters have also been experimentally correlated with elastic mechanical properties using cadaver bone [93–98]. Independent of apparent BMD, bone regions with different architectures exhibited variable elastic mechanical properties that differed by over 50% [59]. Based on studies using two-dimensional serial sectioning techniques, trabecular orientation and connectivity correlated with cancellous bone strength [18, 95, 99]. In sheep femoral bone assessed with micro-CT, architecture indices explained 10–70% of the variation in compressive strength [100]. A study using static histomorphometry indicated that similar architecture–strength correlations also hold true in human vertebral bone [101].

Bone Tissue Material Properties

The intrinsic material properties of bone tissue are important contributors to bone strength and are independent of the quantity or geometric arrangement of the constituent material. Cortical and cancellous tissues are believed to be similar at the material level, both forming lamellar-based structures via surface-based processes, and apparent-level differences between the two are thought to result from contributions of mass and architecture. In bone material tests, the small, homogeneous tissue samples can be loaded perpendicular to the face of the material to determine the tensile and compressive properties or parallel to the face to measure the shear properties. From these tests, bone material properties are computed by normalizing the resulting load-displacement parameters by geometric measures representing the sample size and shape. For example, applied load is converted to tissue stress, and displacement is converted to tissue strain, as described below.

Tissue stress is defined as the ratio of the applied load (tension, compression, or shear) to the sample cross-sectional area (Fig. 10.4). For a tissue sample tested in tension or compression, the tissue stress is defined as the applied load divided by the cross-sectional area perpendicular

to that load (i.e., the area of the sample face on which the load acts). For a tissue sample tested in shear, the applied load is parallel to the surface and again is normalized by the area the force acts across. Bone tissue strain is measured as the amount of deformation in the direction of loading normalized by the initial sample dimension. Tensile or compressive loads produce stretched or compacted deformations, respectively, along the direction of the applied load. The resulting strain is computed as the ratio of the change in length to initial length. Shear loads create distortions in the sample by inducing the sample surfaces on which the loads are applied to slide with respect to each other. For shear strain, the distortion ratio is related to the change in angle, which, for small angles, is approximated by the ratio of the horizontal sliding deformation to the initial length of that side (Fig. 10.4).

The material tests described thus far are for characterizing material behavior in response to a single load applied to failure. In vivo, however, bones continually experience cyclic loading during normal activities, and bone failure from such loading is more common than with a single overloading event [102]. The failure of a material under cyclic loads below the ultimate load is known as fatigue. In bone, fatigue loading produces microscale damage in the tissue, known as microdamage. Microdamage alters bone tissue properties and thus may inhibit the ability of the whole bone to withstand loads and avoid fracture.

Bone is a composite tissue comprised of an organic matrix made mostly of type I collagen that is reinforced by inorganic mineral crystals. The characteristics of these organic and inorganic constituents, as well as their interaction with each other, determine the tissue material properties of bone, properties that at least partially define the popular term *bone quality*. Little is known about the individual and collective contributions of the collagen matrix and mineral constituents to bone quality and bone strength. Indeed, the strength of the composite bone tissue is greater than that of other materials composed primarily of only one of the constituents, such as collagen-rich tendon or mineral samples of calcium phosphate [103].

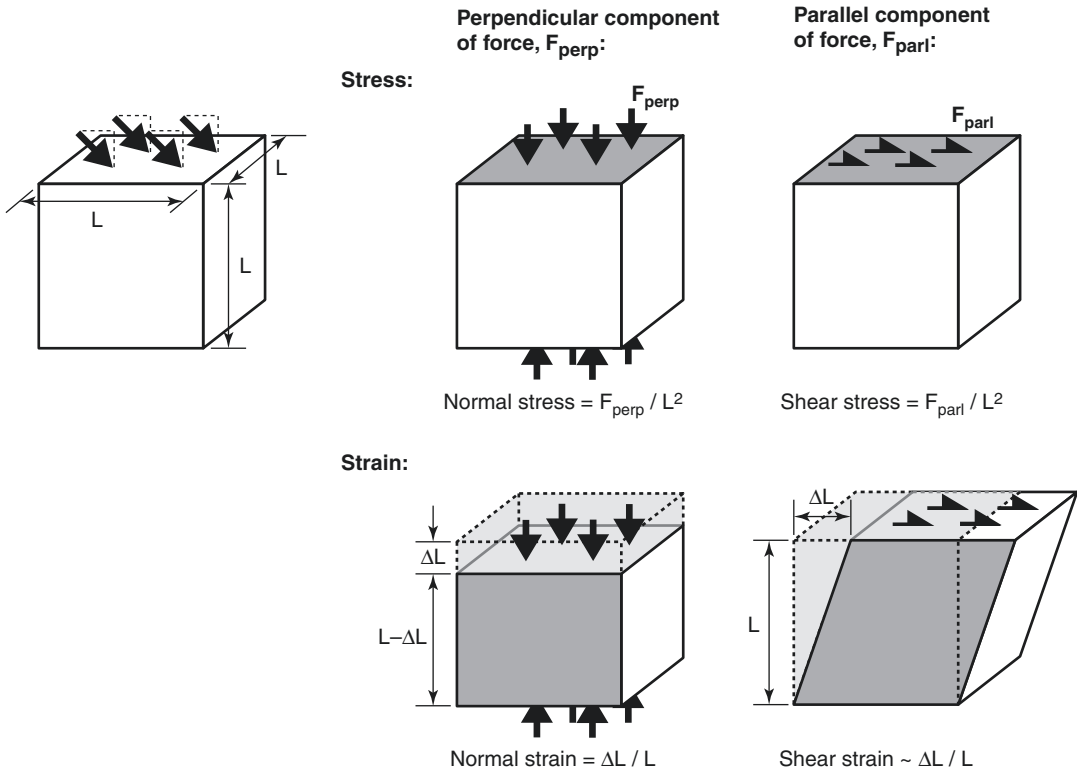


Fig. 10.4 Material stresses (local tissue forces) and strains (local tissue deformations) for bone tissue samples loaded in compression and shear. The applied loading is decomposed into components perpendicular

(compression) and parallel (shear) to the cube face. The face for which the stress or strain is calculated is shaded. For strain, the original, undeformed volume is shaded

Studies of radiation in human bone and allograft specimens revealed that collagen damage compromises the toughness but not the stiffness of bone tissue [104, 105]. In rat bone, when the enzymatic crosslinking in collagen was disrupted through a lysyl oxidase inhibitor, bone strength was reduced without impacting mineralization [106]. Conditions with collagen defects, such as osteogenesis imperfecta, are associated with altered mineralization and bone fragility, as discussed in more detail below. In addition, numerous studies have shown a clear relationship between bone mineral content and material stiffness or strength [107–110]. These results suggest that the collagen and mineral phases of bone tissue contribute differently to its material behavior.

Characterizing the molecular structure of bone tissue is important for examining the relative contributions of the matrix and mineral con-

stituents to the overall material behavior. Important compositional measures of bone matrix include collagen content, maturity, and orientation, as well as the molecular structure of various matrix proteins that aid in mineral crystal formation, binding, and maturation (e.g., osteopontin, osteocalcin, and bone sialoprotein). Important measures for bone mineral include the apatitic crystal size, orientation, and structure, as well as the degree of ion substitution, particularly the substitution of carbonate in the phosphate binding site, within the lattice or on the surface of the mineral crystals. These structural and compositional measures can be quantified using classic techniques such as gravimetry or more sophisticated techniques such as X-ray diffraction, backscattered electron imaging, and infrared (IR), Raman, and nuclear magnetic resonance (NMR) spectroscopies.

Healthy bone tissue properties show substantial variation both spatially [111–113] and temporally [114, 115] even for a given site and species. Materials testing techniques used to examine tissue properties include microbeam testing and nanoindentation. Using microbeam testing, the trabecular tissue modulus ranged from 3.8 to 20.7 GPa and varied depending on the loading mode [31, 116, 117]. The mean tissue modulus assessed by nanoindentation ranged from 7 to 26 GPa, depending on location within the tissue and type of lamellar tissue sampled; individual measurements varied by 17–62% [118–121]. This variation in modulus was true across individuals and for multiple anatomic sites. Even within a single trabecula, the indentation modulus ranged from 8 to 16 GPa [119]. As clearly evidenced by these studies, the variability in measurements of bone tissue properties can be quite large and depends on the technique used. Therefore, the effect of bone tissue composition and distribution on mechanical properties needs further exploration, particularly for cancellous bone. To date, almost all of the techniques used to measure bone material properties directly have been performed *in vitro* and require an invasive bone biopsy. Recent studies have explored the use of an *in vivo* Raman spectroscopic probe that can noninvasively measure bone matrix and mineral composition, although these devices are still in the developmental stages and have not yet been fully validated [122–124].

Other Influences on Bone Biomechanics

Many other factors influence the structural behavior of whole bones and the apparent behavior of cortical and cancellous tissue, including age, sex, and disease. These influences alter bone quantity, geometry/architecture, and tissue properties, all of which govern the mechanical performance of whole bones and bone tissue. For example, with aging, the compressive modulus of vertebral cancellous bone decreases 17% per decade [125]. Osteoporosis and aging are tightly coupled in women, and osteoporosis may in fact be the natural outcome of the aging process.

Aging

The factors described above (i.e., bone quantity, geometry/architecture, and material properties) vary independently with age. Age-related degradation of bone mass and architecture can seriously compromise bone integrity. Bone mass decreases with age after peak bone mass has been attained in both men and women [126–131], but especially in women due to peri-menopausal bone loss. By age 80, aBMD at the common fracture sites of the spine, hip, and forearm decreases by 13–18% in men [132] and 15–54% in women [133–136], thereby increasing the likelihood for developing osteoporosis [137–139]. As the life expectancy of the general population continues to increase, age-related declines will result in even lower bone mass, and the total incidence of skeletal fractures will rise, unless diagnosis and treatment of skeletal deficiencies can be significantly improved [140, 141].

While our understanding of the relationship between tissue composition and material behavior is limited, substantial progress has been made recently in characterizing tissue composition and variation with age. For example, osteons of cortical bone and individual trabeculae of iliac crest biopsies demonstrate spatially varying mineral crystallinity and collagen crosslinking by Fourier transform infrared microscopy [142]. The most crystalline (mature) bone mineral is located at the center of trabeculae, and newly deposited mineral is less crystalline than older mineral. Changes in mineral-to-matrix ratio and mineral maturity are documented with age and disease [143–148]. Femoral heads from patients with hip fractures undergoing total hip arthroplasty demonstrated a significantly increased mineral-to-matrix ratio compared to femoral heads of patients without fractures, suggesting that compositional changes may precede failure [149]. Tissue heterogeneity is known to change with age [150], but studies looking at the relationship between compositional heterogeneity and fracture risk are mixed. In femoral neck biopsies from female hip fracture cases, the compositional heterogeneity (mineral-to-matrix ratio, carbonate-to-phosphate ratio) was lower than in non-fractured controls [151].

However, in iliac crest biopsies from BMD-matched females, compositional heterogeneity (mineral-to-matrix ratio, carbonate-to-phosphate ratio, crystallinity, collagen maturity) was not significantly different between fracture and non-fracture cases [152].

The critical question is how these compositional changes relate to tissue and whole bone mechanical behavior. In rat bone, the mineral-to-matrix ratio, mineral crystallinity, and type-B carbonate substitution were all increased with aging, and these compositional changes were associated with reduced elastic deformation capacity (based on reduced resilience and bending modulus) [153]. Collagen content decreases with age and is associated with reduced post-yield energy dissipation [154]. Age-related accumulation of pentosidine, a marker of advanced glycation endproducts and increased collagen crosslinking, is associated with decreased bone toughness [155]. This accumulation has also been shown to increase matrix protein modifications [156], and advanced glycation end products can predict *in vitro* fracture properties in aged human bone [157]. Clinically, elevated pentosidine levels in urine have been associated with increased fracture incidence in postmenopausal women in the OFELY study [158].

Sex Effects

Given the relatively higher incidence of fragility fractures in women, understanding the sex-related differences in bone quantity, geometry/architecture, and material properties with aging is critical for improved diagnosis and treatment of osteoporosis. For both sexes, volume fraction in human cancellous bone declines steadily throughout life [159–162], as does ash density [125, 163]. However, histomorphometry studies indicated that sex appeared to have minimal or no impact on this relationship [159, 161, 162, 164–166]. Although volume fraction and ash density may change similarly with age for both sexes, similarly altering bone mechanical performance, the mechanisms of bone loss seem to be different and are at least partially related to sex-specific changes

in the cancellous architecture. Regardless of sex, mean trabecular thickness as measured with traditional histomorphometry techniques decreased with age for vertebral bone [160–162, 167]. For men, decreased bone volume resulted more from progressive thinning of trabeculae while maintaining the trabecular network, but for women, bone volume reductions resulted mainly from a loss of trabeculae (and consequently an increase in trabecular separation), while the thickness of the remaining trabeculae was maintained [159].

Interestingly, these sex-specific changes in architecture with age alter the modulus and strength of cancellous bone very differently. When a 10% reduction in bone density was modeled in human vertebral cancellous bone, uniform thinning of trabeculae only reduced the bone strength by 20%, while the random removal of entire trabeculae reduced strength by 70%, and a reduction in both thickness and number reduced strength by 77% [168]. Even when normal bone density was restored by increasing the thickness of trabeculae to compensate for the bone loss, a strength deficit of 63% remained, which may help explain the higher fracture incidence observed clinically in women.

Disease

Although bone is a living tissue that adapts to its mechanical environment, disruptions in bone metabolism by diseases such as osteoporosis and osteogenesis imperfecta can seriously compromise structural integrity and the ability of bone to bear loads. Osteoporosis is a skeletal condition marked by reduced bone mass and a deteriorated architecture, which reduces bone strength and increases the likelihood of fracture [169, 170]. About 50% of white women and 20% of white men over 50 years of age will experience an osteoporotic fracture at the spine, hip, or forearm in their lifetime [170]. For white women, the lifetime risk of hip fracture (1 in 6) is greater than the risk of breast cancer (1 in 9). By 2030, the prevalence of osteoporosis and low bone mass are expected to increase by 30% (relative to 2010 levels) in the United States, increasing from 54

million to over 71 million, thereby increasing fracture rates. Osteoporosis is often asymptomatic prior to fracture, thus making prediction and possible prevention difficult.

In addition to reducing bone mass, osteoporosis also detrimentally affects architecture and material properties. Osteoporotic patients who sustain a vertebral fracture experience more trabecular thinning at the spine and iliac crest than normal, non-fractured aging subjects, resulting in a lower trabecular density, loss of trabecular connectivity, and the disappearance of load-bearing trabecular struts [171, 172]. This architectural disruption from osteoporosis is sometimes accompanied by a compensatory increase in trabecular thickness [171], although this adaptive mechanism does not necessarily prevent fracture. Similarly, at the proximal femur, female patients with hip fractures had a lower bone volume fraction, trabecular number, and connectivity than normal cadaveric controls, and the orientation of the trabecular structure was more aligned with the primary direction of loading, a characteristic known as *structural anisotropy* [173]. The architectural deficits in subjects with osteoporotic fractures were accompanied by reduced bone material stiffness and strength. In addition, bone biopsies of fracture patients revealed changes in tissue composition with osteoporosis, with fracture patients having a lower mineral content, higher crystallinity, and higher collagen maturity than age-matched controls [146, 174].

Often referred to as brittle bone disease, osteogenesis imperfecta (OI) literally means *imperfect bone formation* and is a group of hereditary genetic disorders that primarily affect bone and lead to increased bone fragility. Most commonly OI results from mutations in the genes that encode for type I collagen [175], but mutations in other genes can also result in OI, including those important for collagen modifications preceding crosslinking and fibril formation and those involved in osteoblast differentiation and mineralization (reviewed by [176]). Therefore, most patients with clinical OI (i.e., types I–IV) experience abnormalities in type I collagen, the primary component of the bone tissue matrix, which may alter the normal mineralization process. Bone

strength is compromised in patients with OI, as evidenced by the degradation in bone mass and material properties. Cortical bone in the femora of adult mice with a moderate-to-severe phenotype of OI (*oim/oim*) was significantly weaker than in wild-type mice, and the bone tissue was less compliant and resistant to fracture, as evidenced by reduced moment of inertia, ultimate load, stiffness, energy to failure, ultimate stress, and toughness and increased brittleness [177]. In this mouse model, the mineral-to-matrix ratio was increased, likely due to a lower matrix collagen content [178]. In children and adults with OI types I–IV, bone mineral content and bone size were substantially reduced by 1.6–5.2 standard deviations as compared to normal controls [179, 180]. Matrix collagen defects will adversely affect bone mineral formation and likely compromise bone tissue properties. Therefore, the accurate evaluation of bone strength using surrogate predictions from routine clinical and laboratory assessment tools is essential, as is understanding the determinants of bone mechanical behavior.

Bone Strength Predictions from In Vivo Measurements

Clinical imaging techniques are routinely used to assess bone mass and geometry, and advancements in CT imaging have enabled analyzing cortical and cancellous compartments separately, as well as characterizing spatial distributions of bone mass and geometry and some measures of cancellous architecture. Direct measurements of tissue material properties cannot yet be made noninvasively, although two instruments can measure resistance to microindentation in cortical bone tissue in vivo: BioDent™ and OsteoProbe® (Active Life Scientific, Santa Barbara, CA) [181–183]. This microindentation technology has produced mixed results related to its diagnostic utility. In clinical populations, several studies have reported that the bone material strength index (BMSi) measured in vivo with impact microindentation (OsteoProbe®) at the tibial mid-diaphysis can distinguish between subjects with and without fragility fracture [184–187]. However, in one study,

BMSi was not associated with prevalent fracture in older women (75–80 years old) [188], and in another study, BMSi values were similar across postmenopausal women without fracture and with atypical femoral fracture (AFF) or hip fracture [189]. The BioDent cyclic reference point indentation (RPI) device more consistently discriminated between fracture and non-fracture cases, particularly using indentation distance increase (IDI) measured *in vivo* in the tibia (fragility fractures, AFF) [181, 190] and *ex vivo* in femoral neck tissue extracted from hip fracture patients during surgery [191–193].

Although metrics from both microindentation tools seem to be associated with bone fracture in some studies, they are generally only weakly correlated with a few specific cortical bone material properties, and these relationships have been inconsistent across studies. IDI measured by cyclic RPI was largely independent of age, aBMD by DXA, and cortical geometry by HR-pQCT [194], and it explained only 25–35% of the variation in apparent-level ultimate stress and toughness from bending tests in one study [195], and only 16% in fracture toughness and derived elastic modulus in another study [192]. However, a finite element model of impact microindentation suggested that BMSi is sensitive to changes in material properties, especially elastic modulus and a scalar damage parameter [196]. In terms of composition, one study reported that accumulation of advanced glycation endproducts in collagen and cortical porosity were both correlated positively with IDI and negatively with BMSi [197], although these relationships were also very weak. Collectively, these studies suggest that metrics from cyclic RPI and impact indentation may reflect aspects of both elastic and plastic properties of cortical bone tissue but are not definitely associated with any particular material property. In addition, when cadaveric bone samples were experimentally manipulated (e.g., drying and ashing to reduce toughness), RPI parameters responded differently than traditional material properties from bending tests, challenging the previous notion that IDI was inversely associated with bone toughness [198]. Furthermore, cyclic and impact measurements are only weakly corre-

lated with each other and likely are related to contributions from different bone properties [194]. More extensive testing is needed to understand the clinical utility of these microindentation devices for specific patient populations and their ability to predict fracture in individual patients. These measures may be useful in assessing bone tissue quality locally during implant surgeries, thereby predicting mechanical competence at the interface [199].

Several analytical techniques can be used to extract structural properties from subject-specific images with varying degrees of simplifying assumptions. These structural properties can then be used to predict the strength and fracture risk of skeletal sites that commonly fracture, as well as provide insight into the etiology of fractures. The analytical approaches include structural analyses of densitometric data based on assumed geometric models, and engineering beam theory and finite element (FE) analyses based on CT data. The strength of these methods is that a mechanically meaningful mechanism can be determined to compare the structural performance of bones from different individuals, rather than representing the complex structure with a single bone density value.

The X-ray attenuation profile obtained from DXA can be used to determine geometric properties, including cross-sectional area and polar moment of inertia about a plane perpendicular to the scan direction, assuming that these measures are defined solely by the mineral phase [55, 200–202]. If structural changes in whole bone properties are assumed to arise only from geometric changes and not from alterations in tissue properties, then DXA-derived parameters can also be used to predict structural performance. This method has been applied extensively to the femoral neck and midshaft [200, 203–205], the distal radius [201], and more recently the distal femur [206]. Calculating the structural behavior with this method requires assumptions to determine the underlying geometry, mineral distribution and density, and relative cortical and cancellous fractions; therefore, the application of this technique may be most appropriate for cortical sites.

QCT scans can be analyzed slice-by-slice to examine bone strength indices at sites where most fractures occur clinically, the spine, hip, and forearm [207]. The axial, bending, and torsional rigidity can be calculated in each slice based on composite beam theory [208–210], and assuming bone tissue fails at a constant strain [211], whole bone failure load can be determined as proportional to the minimum structural rigidity in the cross sections. This approach combines appropriate geometric properties of the bone or bone segment (i.e., cross-sectional area for axial tension/compression, moments of inertia for bending and torsion) with the voxel-based values of material properties (i.e., elastic modulus), calculated based on the apparent-level tissue density and empirical equations noted earlier. Model-based estimates of bending and torsional rigidity together were better predictors of fracture than were traditional radiographic methods [212]. Axial rigidity correlated better with experimentally measured vertebral strength than did BMD-based structural measures and was equivalent to finite element strength predictions, at least for this simple compression loading scenario [213, 214]. Historically, CT-based strength indices were used in retrospective population-based studies to compare the mechanical competence of bone in the spine, hip, and wrist across ages and between sexes [215, 216]. More recently, these CT-based methods were applied prospectively to predict incident vertebral and hip fractures in cancer patients with skeletal lesions [217, 218]; however, these studies used the ratio of the affected bone to the contralateral bone to discriminate fracture vs. non-fracture cases, an approach not appropriate for osteoporosis or other conditions that affect both limbs similarly.

Finite element models of the spine and proximal femur take this QCT-based approach further and provide the opportunity to include subject-specific bone geometry, distribution of apparent properties, and more complex loading conditions in a fully three-dimensional analysis [219, 220]. As in the two-dimensional analysis, the bone geometry is modeled with high fidelity from the scan data, and apparent-level material properties can be included based on the CT-measured den-

sity. In contrast to the stiffness determined from the two-dimensional analyses, FE models can predict both stiffness and strength when nonlinear analyses are performed. When FE models of vertebral and femoral bone are compared to ex vivo mechanical testing data, the FE-predicted strength correlates well with the experimentally measured failure strength (explaining 50–95% of the variance) and explains 10–40% more variability in strength than does BMD from DXA or QCT [213, 221–232].

The ability of QCT-derived, specimen-specific FE models to predict vertebral and hip fractures independently of BMD has been examined in two prospective clinical studies, the multi-center osteoporotic fractures in men (MrOS) study with a cohort of ethnically diverse men aged 65 and older [73, 77] and the single-center Age, Gene/Environment Susceptibility-Reykjavik Study (AGES-Reykjavik) consisting of Icelandic men and women born between 1907 and 1935 [76, 233–235]. In the MrOS study, FE vertebral strength predicted fracture independent of lumbar spine (LS) aBMD; and after adjusting for age, race, body mass index (BMI), and clinical center, FE strength was a better predictor of vertebral fracture than LS aBMD but not QCT integral (cortical and cancellous) vBMD [77]. In the AGES-Reykjavik study, after adjusting for age, BMI, and prior fracture, FE vertebral strength was associated with fracture, independent of vBMD, for men but not women [76]. In the proximal femur, strength from the FE models predicted hip fracture in both cohorts [73, 76, 233, 234], although it was not independent of BMD for all cases. In MrOS, after adjusting for age, BMI, clinical center, and total hip aBMD, FE femoral strength was no longer significantly associated with hip fracture [73]. In AGES, after adjusting for age, BMI, and CT-based femoral neck aBMD, FE strength remained associated with hip fracture for women but not for men, and if CT-based total hip aBMD was used in the model instead, FE strength was associated with fracture for both men and women [76].

QCT-based FE models are a promising technique to predict bone strength noninvasively at sites that commonly experience fragility frac-

tures, although they do not yet reliably predict fracture better than BMD in all studies. The predictive ability of these models depends on the specific density-modulus relationships used [236, 237] and may be improved by the use of subject-specific relationships [238]. In addition, most models simulate quasi-static loading conditions and are validated with quasi-static mechanical testing, but recent studies indicate that dynamic FE models that include more sophisticated material mapping strategies, and are validated with more dynamic impact tests simulating falling, may improve model accuracy [239]. In particular, improving our understanding of both cortical and trabecular bone behavior at high strain rates, and the specific loading conditions that lead to fracture, may lead to improved FE models that are more consistently predictive of fracture. Furthermore, higher spatial resolution in CT scans would also improve these models, as spatial variation in geometric and material properties would be captured more accurately [240].

HR-pQCT scans have enabled the development of micro-FE models [241, 242], although this technique is still mostly limited to research studies and can only be done in the peripheral skeleton. Because HR-pQCT scans overestimate bone volume compared with micro-CT (regression slopes of 0.73–0.86 for ex vivo experiments) [26, 243–245], micro-FE models overestimate bone stiffness and strength, which are highly dependent on bone volume fraction. Nevertheless, results from micro-FE models based on HR-pQCT scans are highly correlated with those based on micro-CT scans, and their behavior can be adjusted by altering the tissue modulus or parameters in the failure criterion [241]. Based on ex vivo mechanical testing experiments, micro-FE models from HR-pQCT can accurately predict bone strength in the distal radius and tibia, but results are highly dependent on the modulus and study parameters, which vary across studies [246–250]. In vivo studies showed that FE-predicted properties (e.g., stiffness, strength) at the distal radius and tibia were associated with several types of fragility fractures in men and women [251, 252]. An ex vivo

study similarly found that FE-predicted radius strength correlated with measured L4 vertebral strength and that FE-predicted tibial strength was strongly correlated with both vertebral and femoral strength [253]. However, more studies, and in particular prospective studies, are needed to determine the efficacy of micro-FE calculated strength at peripheral sites in predicting vertebral or hip fractures. In addition, although micro-FE models consistently predict bone strength better than BMD, they do not clearly provide better prediction of fracture risk even at the distal radius [241].

In summary, current clinical tools that assess fracture risk based primarily on bone mass and geometry do not reliably predict whether or not a patient will fracture. Based on the concepts of bone mechanics and laboratory studies presented here, we see that the structure and properties of bones are complex and depend on many factors. Future techniques should combine information regarding an individual's bone mass, geometry/architecture, and tissue material properties to provide a more precise measurement of bone strength and susceptibility to fracture, regardless of age, sex, or the presence of skeletal diseases (and perhaps even more so because of these). A combined imaging–modeling approach can include all of these factors and has the potential to elucidate skeletal structural performance mechanistically and improve our ability to predict skeletal fragility. Recent advances in QCT-based FE modeling and HR-pQCT-based micro-FE modeling show promise for fracture prediction, although more research is needed to improve the accuracy of these models, particularly in terms of more realistic material mapping and mimicking of in vivo loading conditions. Furthermore, fracture risk also depends on the loading environment and the propensity for falling. Improving the accuracy of model boundary conditions through better estimates for the nature and magnitude of mechanical forces experienced during a variety of tasks, and expanding to multi-scale representations that capture other important factors, such as muscle strength and balance, could substantially advance clinical fracture prediction.

References

1. Gabriel SE, Tosteson AN, Leibson CL, Crowson CS, Pond GR, Hammond CS, et al. Direct medical costs attributable to osteoporotic fractures. *Osteoporos Int*. 2002;13(4):323–30.
2. Johnell O. The socioeconomic burden of fractures: today and in the 21st century. *Am J Med*. 1997;103(2A):20S–5S; discussion 5S–6S
3. Melton LJ 3rd. Who has osteoporosis? A conflict between clinical and public health perspectives. *J Bone Miner Res*. 2000;15(12):2309–14.
4. Hayes WC, Piazza SJ, Zysset PK. Biomechanics of fracture risk prediction of the hip and spine by quantitative computed tomography. *Radiol Clin N Am*. 1991;29(1):1–18.
5. van der Meulen MCH, Jepsen KJ, Mikić B. Understanding bone strength: size isn't everything. *Bone*. 2001;29(2):101–4.
6. Duncan RL, Turner CH. Mechanotransduction and the functional response of bone to mechanical strain. *Calcif Tissue Int*. 1995;57(5):344–58.
7. van der Meulen MCH, Huijskes R. Why mechanobiology? A survey article. *J Biomech*. 2002;35(4):401–14.
8. Carter DR. Mechanical loading history and skeletal biology. *J Biomech*. 1987;20:1095–109.
9. Roux W. Der Kampf der Theile im Organismus: ein Beitrag zur Vervollständigung der mechanischen Zweckmässigkeitslehre: W. Engelmann; 1881.
10. Wolff J. Das Gesetz der Transformation der Knochen (The law of bone remodeling). Berlin: Verlag von August Hirschwald; 1892.
11. Scheuren A, Wehrle E, Flohr F, Muller R. Bone mechanobiology in mice: toward single-cell in vivo mechanomics. *Biomech Model Mechanobiol*. 2017;16(6):2017–34.
12. Bergmann G, Graichen F, Rohlmann A. Hip joint loading during walking and running, measured in two patients. *J Biomech*. 1993;26(8):969–90.
13. Kotzar GM, Davy DT, Goldberg VM, Heiple KG, Berilla J, Heiple KG Jr, et al. Telemeterized in vivo hip joint force data: a report on two patients after total hip surgery. *J Orthop Res*. 1991;9(5):621–33.
14. Carter DR, Hayes WC. The compressive behavior of bone as a two-phase porous structure. *J Bone Joint Surg Am*. 1977;59-A:954–62.
15. Goldstein SA. The mechanical properties of trabecular bone: dependence on anatomic location and function. *J Biomech*. 1987;20(11–12):1055–61.
16. Martin RB, Burr DB, Sharkey NA. *Skeletal tissue mechanics*. New York: Springer; 1998.
17. Raux P, Townsend PR, Miegel R, Rose RM, Radin EL. Trabecular architecture of the human patella. *J Biomech*. 1975;8(1):1–7.
18. Townsend PR, Raux P, Rose RM, Miegel RE, Radin EL. The distribution and anisotropy of the stiffness of cancellous bone in the human patella. *J Biomech*. 1975;8(6):363–7.
19. Riggs BL, Wahner HW, Seeman E, Offord KP, Dunn WL, Mazess RB, et al. Changes in bone mineral density of the proximal femur and spine with aging. Differences between the postmenopausal and senile osteoporosis syndromes. *J Clin Invest*. 1982;70(4):716–23.
20. Schuit SC, van der Klift M, Weel AE, de Laet CE, Burger H, Seeman E, et al. Fracture incidence and association with bone mineral density in elderly men and women: the Rotterdam study. *Bone*. 2004;34(1):195–202.
21. Carter DR, Bouxsein ML, Marcus R. New approaches for interpreting projected bone densitometry data. *J Bone Miner Res*. 1992;7(2):137–45.
22. Moro M, Hecker AT, Bouxsein ML, Myers ER. Failure load of thoracic vertebrae correlates with lumbar bone mineral density measured by DXA. *Calcif Tissue Int*. 1995;56(3):206–9.
23. Laib A, Hauselmann HJ, Ruegsegger P. In vivo high resolution 3D-QCT of the human forearm. *Technol Health Care*. 1998;6(5–6):329–37.
24. Burghardt AJ, Pialat JB, Kazakia GJ, Boutroy S, Engelke K, Patsch JM, et al. Multicenter precision of cortical and trabecular bone quality measures assessed by high-resolution peripheral quantitative computed tomography. *J Bone Miner Res*. 2013;28(3):524–36.
25. Manske SL, Zhu Y, Sandino C, Boyd SK. Human trabecular bone microarchitecture can be assessed independently of density with second generation HR-pQCT. *Bone*. 2015;79:213–21.
26. Laib A, Ruegsegger P. Comparison of structure extraction methods for in vivo trabecular bone measurements. *Comput Med Imaging Graph*. 1999;23(2):69–74.
27. Boutroy S, Bouxsein ML, Munoz F, Delmas PD. In vivo assessment of trabecular bone microarchitecture by high-resolution peripheral quantitative computed tomography. *J Clin Endocrinol Metab*. 2005;90(12):6508–15.
28. Goldstein SA, Wilson DL, Sonstegard DA, Matthews LS. The mechanical properties of human tibial trabecular bone as a function of metaphyseal location. *J Biomech*. 1983;16(12):965–9.
29. Gibson LJ. The mechanical behavior of cancellous bone. *J Biomech*. 1985;18:317–28.
30. Hodgkinson R, Currey JD. Young's modulus, density and material properties in cancellous bone over a large density range. *J Mater Sci Mater Med*. 1992;3(5):377–81.
31. Rho JY, Ashman RB, Turner CH. Young's modulus of trabecular and cortical bone material: ultrasonic and microtensile measurements. *J Biomech*. 1993;26(2):111–9.
32. Rice JC, Cowin SC, Bowman JA. On the dependence of the elasticity and strength of cancellous bone on apparent density. *J Biomech*. 1988;21(2):155–68.
33. Snyder SM, Schneider E. Estimation of mechanical properties of cortical bone by computed tomography. *J Orthop Res*. 1991;9(3):422–31.

34. Keaveny TM, Pinilla TP, Crawford RP, Kopperdahl DL, Lou A. Systematic and random errors in compression testing of trabecular bone. *J Orthop Res.* 1997;15(1):101–10.
35. Kopperdahl DL, Keaveny TM. Yield strain behavior of trabecular bone. *J Biomech.* 1998;31(7):601–8.
36. Linde F, Gøthgen CB, Hvid I, Pongsoipetch B. Mechanical properties of trabecular bone by a non-destructive compression testing approach. *Eng Med.* 1988;17(1):23–9.
37. Linde F, Hvid I, Pongsoipetch B. Energy absorptive properties of human trabecular bone specimens during axial compression. *J Orthop Res.* 1989;7(3):432–9.
38. Morgan EF, Bayraktar HH, Keaveny TM. Trabecular bone modulus-density relationships depend on anatomic site. *J Biomech.* 2003;36(7):897–904.
39. Broy SB, Cauley JA, Lewiecki ME, Schousboe JT, Shepherd JA, Leslie WD. Fracture risk prediction by Non-BMD DXA measures: the 2015 ISCD official positions part 1: hip geometry. *J Clin Densitom.* 2015;18(3):287–308.
40. Leslie WD, Krieg MA, Hans D. Clinical factors associated with trabecular bone score. *J Clin Densitom.* 2013;16(3):374–9.
41. Faulkner KG, Cummings SR, Black D, Palermo L, Gluer CC, Genant HK. Simple measurement of femoral geometry predicts hip fracture: the study of osteoporotic fractures. *J Bone Miner Res.* 1993;8(10):1211–7.
42. Leslie WD, Lix LM, Morin SN, Johansson H, Oden A, McCloskey EV, et al. Hip axis length is a FRAX- and bone density-independent risk factor for hip fracture in women. *J Clin Endocrinol Metab.* 2015;100(5):2063–70.
43. Leslie WD, Lix LM, Morin SN, Johansson H, Oden A, McCloskey EV, et al. Adjusting hip fracture probability in men and women using hip axis length: the Manitoba bone density database. *J Clin Densitom.* 2016;19(3):326–31.
44. Kanis JA, Johnell O, Oden A, Johansson H, McCloskey E. FRAX and the assessment of fracture probability in men and women from the UK. *Osteoporos Int.* 2008;19(4):385–97.
45. Pothuau L, Carceller P, Hans D. Correlations between grey-level variations in 2D projection images (TBS) and 3D microarchitecture: applications in the study of human trabecular bone microarchitecture. *Bone.* 2008;42(4):775–87.
46. Boutroy S, Hans D, Sornay-Rendu E, Vilayphiou N, Winzenrieth R, Chapurlat R. Trabecular bone score improves fracture risk prediction in non-osteoporotic women: the OFELY study. *Osteoporos Int.* 2013;24(1):77–85.
47. Briot K, Paternotte S, Kolta S, Eastell R, Reid DM, Felsenberg D, et al. Added value of trabecular bone score to bone mineral density for prediction of osteoporotic fractures in postmenopausal women: the OPUS study. *Bone.* 2013;57(1):232–6.
48. Hans D, Goertzen AL, Krieg MA, Leslie WD. Bone microarchitecture assessed by TBS predicts osteoporotic fractures independent of bone density: the Manitoba study. *J Bone Miner Res.* 2011;26(11):2762–9.
49. Iki M, Tamaki J, Kadowaki E, Sato Y, Dongmei N, Winzenrieth R, et al. Trabecular bone score (TBS) predicts vertebral fractures in Japanese women over 10 years independently of bone density and prevalent vertebral deformity: the Japanese Population-Based Osteoporosis (JPOS) cohort study. *J Bone Miner Res.* 2014;29(2):399–407.
50. Lamy O, Metzger M, Krieg MA, Aubry-Rozier B, Stoll D, Hans D. La cohorte OstéoLaus: évaluation des outils de routine clinique pour la prédiction de la fracture ostéoporotique [OsteoLaus: prediction of osteoporotic fractures by clinical risk factors and DXA, IVA and TBS]. *Rev Med Suisse.* 2011;7(315):2130, 2132–4, 2136.
51. Leslie WD, Aubry-Rozier B, Lix LM, Morin SN, Majumdar SR, Hans D. Spine bone texture assessed by trabecular bone score (TBS) predicts osteoporotic fractures in men: the Manitoba Bone Density Program. *Bone.* 2014;67:10–4.
52. Silva BC, Leslie WD. Trabecular bone score: a new DXA-derived measurement for fracture risk assessment. *Endocrinol Metab Clin N Am.* 2017;46(1):153–80.
53. McCloskey EV, Oden A, Harvey NC, Leslie WD, Hans D, Johansson H, et al. A meta-analysis of trabecular bone score in fracture risk prediction and its relationship to FRAX. *J Bone Miner Res.* 2016;31(5):940–8.
54. Roux JP, Wegrzyn J, Boutroy S, Bouxsein ML, Hans D, Chapurlat R. The predictive value of trabecular bone score (TBS) on whole lumbar vertebrae mechanics: an ex vivo study. *Osteoporos Int.* 2013;24(9):2455–60.
55. Martin RB, Burr DB. Non-invasive measurement of long bone cross-sectional moment of inertia by photon absorptiometry. *J Biomech.* 1984;17(3):195–201.
56. Hibbeler RC. *Mechanics of materials.* Upper Saddle River, New Jersey: Prentice Hall; 1997.
57. Cooper A. *A treatise on dislocations and fractures of the joints.* London: Longman, Hurst, Rees, Orme, and Brown; 1842.
58. Galante J, Rostoker W, Ray RD. Physical properties of trabecular bone. *Calcif Tissue Res.* 1970;5:236–46.
59. Ulrich D, Hildebrand T, van Rietbergen B, Müller R, Rügsegger P. The quality of trabecular bone evaluated with micro-computed tomography, FEA and mechanical testing. *Stud Health Technol Inform.* 1997;40:97–112.
60. Mosekilde L. Consequences of the remodelling process for vertebral trabecular bone structure: a scanning electron microscopy study (uncoupling of unloaded structures). *Bone Miner.* 1990;10(1):13–35.
61. Hans D, Barthe N, Boutroy S, Pothuau L, Winzenrieth R, Krieg MA. Correlations between trabecular bone score, measured using anteroposterior dual-energy X-ray absorptiometry acquisition, and 3-dimensional parameters of bone microarchitecture: an experimental study on human cadaver vertebrae. *J Clin Densitom.* 2011;14(3):302–12.

62. Muschitz C, Kocijan R, Haschka J, Pahr D, Kaider A, Pietschmann P, et al. TBS reflects trabecular microarchitecture in premenopausal women and men with idiopathic osteoporosis and low-traumatic fractures. *Bone*. 2015;79:259–66.
63. Popp AW, Buffat H, Eberli U, Lippuner K, Ernst M, Richards RG, et al. Microstructural parameters of bone evaluated using HR-pQCT correlate with the DXA-derived cortical index and the trabecular bone score in a cohort of randomly selected premenopausal women. *PLoS One*. 2014;9(2):e88946.
64. Silva BC, Boutroy S, Zhang C, McMahon DJ, Zhou B, Wang J, et al. Trabecular bone score (TBS)—a novel method to evaluate bone microarchitectural texture in patients with primary hyperparathyroidism. *J Clin Endocrinol Metab*. 2013;98(5):1963–70.
65. Winzenrieth R, Michelet F, Hans D. Three-dimensional (3D) microarchitecture correlations with 2D projection image gray-level variations assessed by trabecular bone score using high-resolution computed tomographic acquisitions: effects of resolution and noise. *J Clin Densitom*. 2013;16(3):287–96.
66. Black DM, Bouxsein ML, Marshall LM, Cummings SR, Lang TF, Cauley JA, et al. Proximal femoral structure and the prediction of hip fracture in men: a large prospective study using QCT. *J Bone Miner Res*. 2008;23(8):1326–33.
67. Borggreffe J, de Buhr T, Shrestha S, Marshall LM, Orwoll E, Peters K, et al. Association of 3D geometric measures derived from quantitative computed tomography with hip fracture risk in older men. *J Bone Miner Res*. 2016;31(8):1550–8.
68. Bredbenner TL, Mason RL, Havill LM, Orwoll ES, Nicolella DP. Fracture risk predictions based on statistical shape and density modeling of the proximal femur. *J Bone Miner Res*. 2014;29(9):2090–100.
69. Carballido-Gamio J, Harnish R, Saeed I, Streeper T, Sigurdsson S, Amin S, et al. Proximal femoral density distribution and structure in relation to age and hip fracture risk in women. *J Bone Miner Res*. 2013;28(3):537–46.
70. Carballido-Gamio J, Harnish R, Saeed I, Streeper T, Sigurdsson S, Amin S, et al. Structural patterns of the proximal femur in relation to age and hip fracture risk in women. *Bone*. 2013;57(1):290–9.
71. Chalhoub D, Orwoll ES, Cawthon PM, Ensrud KE, Boudreau R, Greenspan S, et al. Areal and volumetric bone mineral density and risk of multiple types of fracture in older men. *Bone*. 2016;92:100–6.
72. Johannesdottir F, Poole KE, Reeve J, Siggeirsdottir K, Aspelund T, Mogensen B, et al. Distribution of cortical bone in the femoral neck and hip fracture: a prospective case-control analysis of 143 incident hip fractures; The AGES-REYKJAVIK Study. *Bone*. 2011;48(6):1268–76.
73. Orwoll ES, Marshall LM, Nielson CM, Cummings SR, Lapidus J, Cauley JA, et al. Finite element analysis of the proximal femur and hip fracture risk in older men. *J Bone Miner Res*. 2009;24(3):475–83.
74. Treece GM, Gee AH, Tonkin C, Ewing SK, Cawthon PM, Black DM, et al. Predicting hip fracture type with cortical bone mapping (CBM) in the osteoporotic fractures in men (MrOS) study. *J Bone Miner Res*. 2015;30(11):2067–77.
75. Yang L, Burton AC, Bradburn M, Nielson CM, Orwoll ES, Eastell R, et al. Distribution of bone density in the proximal femur and its association with hip fracture risk in older men: the osteoporotic fractures in men (MrOS) study. *J Bone Miner Res*. 2012;27(11):2314–24.
76. Kopperdahl DL, Aspelund T, Hoffmann PF, Sigurdsson S, Siggeirsdottir K, Harris TB, et al. Assessment of incident spine and hip fractures in women and men using finite element analysis of CT scans. *J Bone Miner Res*. 2014;29(3):570–80.
77. Wang X, Sanyal A, Cawthon PM, Palermo L, Jekir M, Christensen J, et al. Prediction of new clinical vertebral fractures in elderly men using finite element analysis of CT scans. *J Bone Miner Res*. 2012;27(4):808–16.
78. Burghardt AJ, Buie HR, Laib A, Majumdar S, Boyd SK. Reproducibility of direct quantitative measures of cortical bone microarchitecture of the distal radius and tibia by HR-pQCT. *Bone*. 2010;47(3):519–28.
79. Vico L, Zouch M, Amirouche A, Frere D, Laroche N, Koller B, et al. High-resolution pQCT analysis of the distal radius and tibia discriminates patients with recent wrist and femoral neck fractures. *J Bone Miner Res*. 2008;23(11):1741–50.
80. Cheung AM, Adachi JD, Hanley DA, Kendler DL, Davison KS, Josse R, et al. High-resolution peripheral quantitative computed tomography for the assessment of bone strength and structure: a review by the Canadian Bone Strength Working Group. *Curr Osteoporos Rep*. 2013;11(2):136–46.
81. Liu XS, Shane E, McMahon DJ, Guo XE. Individual trabecula segmentation (ITS)-based morphological analysis of microscale images of human tibial trabecular bone at limited spatial resolution. *J Bone Miner Res*. 2011;26(9):2184–93.
82. Sornay-Rendu E, Boutroy S, Duboeuf F, Chapurlat RD. Bone microarchitecture assessed by HR-pQCT as predictor of fracture risk in postmenopausal women: the OFELY study. *J Bone Miner Res*. 2017;32(6):1243–51.
83. Carballido-Gamio J, Nicolella DP. Computational anatomy in the study of bone structure. *Curr Osteoporos Rep*. 2013;11(3):237–45.
84. Li W, Kezele I, Collins DL, Zijdenbos A, Keyak J, Kornak J, et al. Voxel-based modeling and quantification of the proximal femur using inter-subject registration of quantitative CT images. *Bone*. 2007;41(5):888–95.
85. Li W, Kornak J, Harris T, Keyak J, Li C, Lu Y, et al. Identify fracture-critical regions inside the proximal femur using statistical parametric mapping. *Bone*. 2009;44(4):596–602.
86. Poole KE, Treece GM, Mayhew PM, Vaculik J, Dungl P, Horak M, et al. Cortical thickness mapping to identify focal osteoporosis in patients with hip fracture. *PLoS One*. 2012;7(6):e38466.

87. Allison SJ, Poole KE, Treece GM, Gee AH, Tonkin C, Rennie WJ, et al. The influence of high-impact exercise on cortical and trabecular bone mineral content and 3D distribution across the proximal femur in older men: a randomized controlled unilateral intervention. *J Bone Miner Res.* 2015;30(9):1709–16.
88. Poole KE, Treece GM, Gee AH, Brown JP, McClung MR, Wang A, et al. Denosumab rapidly increases cortical bone in key locations of the femur: a 3D bone mapping study in women with osteoporosis. *J Bone Miner Res.* 2015;30(1):46–54.
89. Seeherman HJ, Li XJ, Smith E, Parkington J, Li R, Wozney JM. Intraosseous injection of rhBMP-2/calcium phosphate matrix improves bone structure and strength in the proximal aspect of the femur in chronic ovariectomized nonhuman primates. *J Bone Joint Surg Am.* 2013;95(1):36–47.
90. Whitmarsh T, Treece GM, Gee AH, Poole KE. Mapping bone changes at the proximal femoral cortex of postmenopausal women in response to alendronate and teriparatide alone, combined or sequentially. *J Bone Miner Res.* 2015;30(7):1309–18.
91. Nicoletta DP, Bredbenner TL. Development of a parametric finite element model of the proximal femur using statistical shape and density modeling. *Comput Methods Biomech Biomed Engin.* 2012;15(2):101–10.
92. Treece GM, Poole KE, Gee AH. Imaging the femoral cortex: thickness, density and mass from clinical CT. *Med Image Anal.* 2012;16(5):952–65.
93. Cowin SC. The relationship between the elasticity tensor and the fabric tensor. *Mech Mater.* 1985;4:137–47.
94. Goldstein SA, Goulet R, McCubbrey D. Measurement and significance of three-dimensional architecture to the mechanical integrity of trabecular bone. *Calcif Tissue Int.* 1993;53:S127–32; discussion S32–3
95. Goulet RW, Goldstein SA, Ciarelli MJ, Kuhn JL, Brown MB, Feldkamp LA. The relationship between the structural and orthogonal compressive properties of trabecular bone. *J Biomech.* 1994;27(4):375–89.
96. Kabel J, Odgaard A, van Rietbergen B, Huiskes R. Connectivity and the elastic properties of cancellous bone. *Bone.* 1999;24(2):115–20.
97. Odgaard A, Kabel J, van Rietbergen B, Dalstra M, Huiskes R. Fabric and elastic principal directions of cancellous bone are closely related. *J Biomech.* 1997;30(5):487–95.
98. van Rietbergen B, Majumdar S, Pistoia W, Newitt DC, Kothari M, Laib A, et al. Assessment of cancellous bone mechanical properties from micro-FE models based on micro-CT, pQCT and MR images. *Technol Health Care.* 1998;6(5–6):413–20.
99. Pugh JW, Rose RM, Radin EL. A structural model for the mechanical behavior of trabecular bone. *J Biomech.* 1973;6(6):657–70.
100. Mittra E, Rubin C, Qin YX. Interrelationship of trabecular mechanical and microstructural properties in sheep trabecular bone. *J Biomech.* 2005;38(6):1229–37.
101. Thomsen JS, Ebbesen EN, Mosekilde L. Predicting human vertebral bone strength by vertebral static histomorphometry. *Bone.* 2002;30(3):502–8.
102. Burr DB, Forwood MR, Fyhrie DP, Martin RB, Schaffler MB, Turner CH. Bone microdamage and skeletal fragility in osteoporotic and stress fractures. *J Bone Miner Res.* 1997;12(1):6–15.
103. Currey JD. Role of collagen and other organics in the mechanical properties of bone. *Osteoporos Int.* 2003;14(Suppl 5):S29–36.
104. Currey JD, Foreman J, Laketic I, Mitchell J, Pegg DE, Reilly GC. Effects of ionizing radiation on the mechanical properties of human bone. *J Orthop Res.* 1997;15(1):111–7.
105. Hamer AJ, Stockley I, Elson RA. Changes in allograft bone irradiated at different temperatures. *J Bone Joint Surg Br.* 1999;81(2):342–4.
106. Oxlund H, Barckman M, Ortoft G, Andreassen TT. Reduced concentrations of collagen cross-links are associated with reduced strength of bone. *Bone.* 1995;17(4 Suppl):365S–71S.
107. Burstein AH, Zika JM, Heiple K, Klein L. Contribution of collagen and mineral to the elastic-plastic properties of bone. *J Bone Joint Surg Am.* 1975;57(7):956–61.
108. Currey JD. The effect of porosity and mineral content on the Young's modulus of elasticity of compact bone. *J Biomech.* 1988;21(2):131–9.
109. Currey JD. What determines the bending strength of compact bone? *J Exp Biol.* 1999;202(Pt 18):2495–503.
110. Martin RB, Boardman DL. The effects of collagen fiber orientation, porosity, density, and mineralization on bovine cortical bone bending properties. *J Biomech.* 1993;26(9):1047–54.
111. Bonucci E, Ballanti P, Della Rocca C, Milani S, Lo Cascio V, Imbimbo B. Technical variability of bone histomorphometric measurements. *Bone Miner.* 1990;11(2):177–86.
112. Malluche HH, Meyer W, Sherman D, Massry SG. Quantitative bone histology in 84 normal American subjects. Micromorphometric analysis and evaluation of variance in iliac bone. *Calcif Tissue Int.* 1982;34(5):449–55.
113. Ninomiya JT, Tracy RP, Calore JD, Gendreau MA, Kelm RJ, Mann KG. Heterogeneity of human bone. *J Bone Miner Res.* 1990;5(9):933–8.
114. Handschin RG, Stern WB. Crystallographic and chemical analysis of human bone apatite (Crista Iliaca). *Clin Rheumatol.* 1994;13(Suppl 1):75–90.
115. Handschin RG, Stern WB. X-ray diffraction studies on the lattice perfection of human bone apatite (Crista iliaca). *Bone.* 1995;16(4 Suppl):355S–63S.
116. Choi K, Kuhn JL, Ciarelli MJ, Goldstein SA. The elastic moduli of human subchondral, trabecular, and cortical bone tissue and the size-dependency of cortical bone modulus. *J Biomech.* 1990;23(11):1103–13.

117. Kuhn JL, Goldstein SA, Choi K, London M, Feldkamp LA, Matthews LS. Comparison of the trabecular and cortical tissue moduli from human iliac crests. *J Orthop Res.* 1989;7(6):876–84.
118. Rho JY, Roy ME 2nd, Tsui TY, Pharr GM. Elastic properties of microstructural components of human bone tissue as measured by nanoindentation. *J Biomed Mater Res.* 1999;45(1):48–54.
119. Rho JY, Tsui TY, Pharr GM. Elastic properties of human cortical and trabecular lamellar bone measured by nanoindentation. *Biomaterials.* 1997;18(20):1325–30.
120. Turner CH, Rho J, Takano Y, Tsui TY, Pharr GM. The elastic properties of trabecular and cortical bone tissues are similar: results from two microscopic measurement techniques. *J Biomech.* 1999;32(4):437–41.
121. Zysset PK, Guo XE, Hoffler CE, Moore KE, Goldstein SA. Elastic modulus and hardness of cortical and trabecular bone lamellae measured by nanoindentation in the human femur. *J Biomech.* 1999;32(10):1005–12.
122. Matousek P, Draper ER, Goodship AE, Clark IP, Ronayne KL, Parker AW. Noninvasive Raman spectroscopy of human tissue in vivo. *Appl Spectrosc.* 2006;60(7):758–63.
123. Schulmerich MV, Cole JH, Kreider JM, Esmonde-White F, Dooley KA, Goldstein SA, et al. Transcutaneous Raman spectroscopy of murine bone in vivo. *Appl Spectrosc.* 2009;63(3):286–95.
124. Shu C, Chen K, Lynch M, Maher JR, Awad HA, Berger AJ. Spatially offset Raman spectroscopy for in vivo bone strength prediction. *Biomed Opt Express.* 2018;9(10):4781–91.
125. Mosekilde L, Mosekilde L, Danielsen CC. Biomechanical competence of vertebral trabecular bone in relation to ash density and age in normal individuals. *Bone.* 1987;8(2):79–85.
126. (None). Bone density reference data. In: Favus MJ, editor. *Primer on the metabolic bone diseases and disorders of mineral metabolism.* 4th ed. Philadelphia: Lippincott Williams & Wilkins; 1996. p. 483.
127. Barden H. Bone mineral density of the spine and femur in normal U.S. white females. *J Bone Miner Res.* 1997;12(Suppl. 1):S248.
128. Diaz Curiel M, Carrasco de la Peña JL, Honorato Perez J, Perez Cano R, Rapado A, Ruiz Martinez I. Study of bone mineral density in lumbar spine and femoral neck in a Spanish population. Multicentre Research Project on Osteoporosis. *Osteoporos Int.* 1997;7(1):59–64.
129. Lehmann R, Wapniarz M, Randerath O, Kvasnicka HM, John W, Reincke M, et al. Dual-energy X-ray absorptiometry at the lumbar spine in German men and women: a cross-sectional study. *Calcif Tissue Int.* 1995;56(5):350–4.
130. Löfman O, Larsson L, Ross I, Toss G, Berglund K. Bone mineral density in normal Swedish women. *Bone.* 1997;20(2):167–74.
131. Vega E, Bagur A, Mautalen CA. Densidad mineral ósea en mujeres osteoporóticas y normales de Buenos Aires. *Medicina.* 1993;53(3):211–6.
132. Szulc P, Munoz F, Duboeuf F, Marchand F, Delmas PD. Bone mineral density predicts osteoporotic fractures in elderly men: the MINOS study. *Osteoporos Int.* 2005;16(10):1184–92.
133. Ahlborg HG, Johnell O, Turner CH, Rannevik G, Karlsson MK. Bone loss and bone size after menopause. *N Engl J Med.* 2003;349(4):327–34.
134. Aloia JF, Vaswani A, Mikhail M, Badshah M, Flaster E. Cancellous bone of the spine is greater in black women. *Calcif Tissue Int.* 1999;65(1):29–33.
135. Arlot ME, Sornay-Rendu E, Garnero P, Vey-Marty B, Delmas PD. Apparent pre- and postmenopausal bone loss evaluated by DXA at different skeletal sites in women: the OFELY cohort. *J Bone Miner Res.* 1997;12(4):683–90.
136. Riggs BL, Khosla S, Melton LJ 3rd. Sex steroids and the construction and conservation of the adult skeleton. *Endocr Rev.* 2002;23(3):279–302.
137. Hui SL, Slemenda CW, Johnston CC Jr. Age and bone mass as predictors of fracture in a prospective study. *J Clin Invest.* 1988;81(6):1804–9.
138. Ross PD, Davis JW, Epstein RS, Wasnich RD. Pre-existing fractures and bone mass predict vertebral fracture incidence in women. *Ann Intern Med.* 1991;114(11):919–23.
139. Ross PD, Davis JW, Vogel JM, Wasnich RD. A critical review of bone mass and the risk of fractures in osteoporosis. *Calcif Tissue Int.* 1990;46(3):149–61.
140. Melton LJ 3rd. Hip fractures: a worldwide problem today and tomorrow. *Bone.* 1993;14:S1–8.
141. National Osteoporosis Foundation. *America's bone health: the state of osteoporosis and low bone mass in our nation.* Washington, D.C: National Osteoporosis Foundation; 2002.
142. Paschalis EP, Betts F, DiCarlo E, Mendelsohn R, Boskey AL. FTIR microspectroscopic analysis of normal human cortical and trabecular bone. *Calcif Tissue Int.* 1997;61(6):480–6.
143. Boskey AL, DiCarlo E, Paschalis E, West P, Mendelsohn R. Comparison of mineral quality and quantity in iliac crest biopsies from high- and low-turnover osteoporosis: an FT-IR microspectroscopic investigation. *Osteoporos Int.* 2005;16(12):2031–8.
144. Kozloff KM, Carden A, Bergwitz C, Forlino A, Uveges TE, Morris MD, et al. Brittle IV mouse model for osteogenesis imperfecta IV demonstrates postpubertal adaptations to improve whole bone strength. *J Bone Miner Res.* 2004;19(4):614–22.
145. Ou-Yang H, Paschalis EP, Mayo WE, Boskey AL, Mendelsohn R. Infrared microscopic imaging of bone: spatial distribution of CO₃(2-). *J Bone Miner Res.* 2001;16(5):893–900.
146. Paschalis EP, Betts F, DiCarlo E, Mendelsohn R, Boskey AL. FTIR microspectroscopic analysis of human iliac crest biopsies from untreated osteoporotic bone. *Calcif Tissue Int.* 1997;61(6):487–92.
147. Tarnowski CP, Ignelzi MA Jr, Morris MD. Mineralization of developing mouse calvaria as revealed by Raman microspectroscopy. *J Bone Miner Res.* 2002;17(6):1118–26.

148. Kim G, Cole JH, Boskey AL, Baker SP, van der Meulen MC. Reduced tissue-level stiffness and mineralization in osteoporotic cancellous bone. *Calcif Tissue Int.* 2014;95(2):125–31.
149. McCreddie BR, Morris MD, Chen TC, Sudhaker Rao D, Finney WF, Widjaja E, et al. Bone tissue compositional differences in women with and without osteoporotic fracture. *Bone.* 2006;39(6):1190–5.
150. Yerramshetty JS, Lind C, Akkus O. The compositional and physicochemical homogeneity of male femoral cortex increases after the sixth decade. *Bone.* 2006;39(6):1236–43.
151. Gourion-Arsiquaud S, Lukashova L, Power J, Loveridge N, Reeve J, Boskey AL. Fourier transform infrared imaging of femoral neck bone: reduced heterogeneity of mineral-to-matrix and carbonate-to-phosphate and more variable crystallinity in treatment-naïve fracture cases compared with fracture-free controls. *J Bone Miner Res.* 2013;28(1):150–61.
152. Boskey AL, Donnelly E, Boskey E, Spevak L, Ma Y, Zhang W, et al. Examining the relationships between bone tissue composition, compositional heterogeneity, and fragility fracture: a matched case-controlled FTIR study. *J Bone Miner Res.* 2016;31(5):1070–81.
153. Akkus O, Adar F, Schaffler MB. Age-related changes in physicochemical properties of mineral crystals are related to impaired mechanical function of cortical bone. *Bone.* 2004;34(3):443–53.
154. Nyman JS, Roy A, Tyler JH, Acuna RL, Gayle HJ, Wang X. Age-related factors affecting the postyield energy dissipation of human cortical bone. *J Orthop Res.* 2007;25(5):646–55.
155. Wang X, Shen X, Li X, Agrawal CM. Age-related changes in the collagen network and toughness of bone. *Bone.* 2002;31(1):1–7.
156. Sroga GE, Karim L, Colon W, Vashishth D. Biochemical characterization of major bone-matrix proteins using nanoscale-size bone samples and proteomics methodology. *Mol Cell Proteomics.* 2011;10(9):M110 006718.
157. Tang SY, Zeenath U, Vashishth D. Effects of non-enzymatic glycation on cancellous bone fragility. *Bone.* 2007;40(4):1144–51.
158. Gineys E, Munoz F, Bertholon C, Sornay-Rendu E, Chapurlat R. Urinary levels of pentosidine and the risk of fracture in postmenopausal women: the OFELY study. *Osteoporos Int.* 2010;21(2):243–50.
159. Aaron JE, Makins NB, Sagreya K. The microanatomy of trabecular bone loss in normal aging men and women. *Clin Orthop Relat Res.* 1987;215:260–71.
160. Dempster DW, Ferguson-Pell MW, Mellish RW, Cochran GV, Xie F, Fey C, et al. Relationships between bone structure in the iliac crest and bone structure and strength in the lumbar spine. *Osteoporos Int.* 1993;3(2):90–6.
161. Mosekilde L. Sex differences in age-related loss of vertebral trabecular bone mass and structure – biomechanical consequences. *Bone.* 1989;10:425–32.
162. Thomsen JS, Ebbesen EN, Mosekilde L. A new method of comprehensive static histomorphometry applied on human lumbar vertebral cancellous bone. *Bone.* 2000;27(1):129–38.
163. Mosekilde L, Mosekilde L. Sex differences in age-related changes in vertebral body size, density and biomechanical competence in normal individuals. *Bone.* 1990;11:67–73.
164. Bergot C, Laval-Jeantet AM, Preteux F, Meunier A. Measurement of anisotropic vertebral trabecular bone loss during aging by quantitative image analysis. *Calcif Tissue Int.* 1988;43(3):143–9.
165. Dunnill MS, Anderson JA, Whitehead R. Quantitative histological studies on age changes in bone. *J Pathol.* 1967;94(2):275–91.
166. Weaver JK, Chalmers J. Cancellous bone: its strength and changes with aging and an evaluation of some methods for measuring its mineral content. *J Bone Joint Surg Am.* 1966;48(2):289–98.
167. Hildebrand T, Laib A, Müller R, Dequeker J, Rüegsegger P. Direct three-dimensional morphometric analysis of human cancellous bone: microstructural data from spine, femur, iliac crest, and calcaneus. *J Bone Miner Res.* 1999;14(7):1167–74.
168. Silva MJ, Gibson LJ. Modeling the mechanical behavior of vertebral trabecular bone: effects of age-related changes in microstructure. *Bone.* 1997;21(2):191–9.
169. Cummings SR, Melton LJ. Epidemiology and outcomes of osteoporotic fractures. *Lancet.* 2002;359(9319):1761–7.
170. US Department of Health and Human Services. Bone health and osteoporosis: a report of the surgeon general. Rockville, MD: U.S. Department of Health and Human Services, Office of the Surgeon General; 2004.
171. Kleerekoper M, Villanueva AR, Stanciu J, Rao DS, Parfitt AM. The role of three-dimensional trabecular microstructure in the pathogenesis of vertebral compression fractures. *Calcif Tissue Int.* 1985;37(6):594–7.
172. Parfitt AM, Mathews CH, Villanueva AR, Kleerekoper M, Frame B, Rao DS. Relationships between surface, volume, and thickness of iliac trabecular bone in aging and in osteoporosis. Implications for the micro-anatomic and cellular mechanisms of bone loss. *J Clin Invest.* 1983;72(4):1396–409.
173. Ciarelli TE, Fyhrie DP, Schaffler MB, Goldstein SA. Variations in three-dimensional cancellous bone architecture of the proximal femur in female hip fractures and in controls. *J Bone Miner Res.* 2000;15(1):32–40.
174. Gadeleta SJ, Boskey AL, Paschalis E, Carlson C, Menschik F, Baldini T, et al. A physical, chemical, and mechanical study of lumbar vertebrae from normal, ovariectomized, and nandrolone decanoate-treated cynomolgus monkeys (*Macaca fascicularis*). *Bone.* 2000;27(4):541–50.
175. Cole WG. Osteogenesis imperfecta. *Bailliere Clin Endocrinol Metab.* 1988;2(1):243–65.
176. Lim J, Grafe I, Alexander S, Lee B. Genetic causes and mechanisms of Osteogenesis Imperfecta. *Bone.* 2017;102:40–9.

177. Misof BM, Roschger P, Baldini T, Raggio CL, Zraick V, Root L, et al. Differential effects of alendronate treatment on bone from growing osteogenesis imperfecta and wild-type mouse. *Bone*. 2005;36(1):150–8.
178. Camacho NP, Landis WJ, Boskey AL. Mineral changes in a mouse model of osteogenesis imperfecta detected by Fourier transform infrared microscopy. *Connect Tissue Res*. 1996;35(1–4):259–65.
179. Kurtz D, Morrish K, Shapiro J. Vertebral bone mineral content in osteogenesis imperfecta. *Calcif Tissue Int*. 1985;37(1):14–8.
180. Lund AM, Molgaard C, Muller J, Skovby F. Bone mineral content and collagen defects in osteogenesis imperfecta. *Acta Paediatr*. 1999;88(10):1083–8.
181. Diez-Perez A, Güerri R, Nagues X, Cáceres E, Peña MJ, Mellibovsky L, et al. Microindentation for in vivo measurement of bone tissue mechanical properties in humans. *J Bone Miner Res*. 2010;25(8):1877–85.
182. Allen MR, McNerny EM, Organ JM, Wallace JM. True gold or pyrite: a review of reference point indentation for assessing bone mechanical properties in vivo. *J Bone Miner Res*. 2015;30(9):1539–50.
183. Farr JN, Drake MT, Amin S, Melton LJ 3rd, McCready LK, Khosla S. In vivo assessment of bone quality in postmenopausal women with type 2 diabetes. *J Bone Miner Res*. 2014;29(4):787–95.
184. Malgo F, Hamdy NA, Papapoulos SE, Appelman-Dijkstra NM. Bone material strength as measured by microindentation in vivo is decreased in patients with fragility fractures independently of bone mineral density. *J Clin Endocrinol Metab*. 2015;100(5):2039–45.
185. Malgo F, Hamdy NAT, Papapoulos SE, Appelman-Dijkstra NM. Bone material strength index as measured by impact microindentation is low in patients with fractures irrespective of fracture site. *Osteoporos Int*. 2017;28(8):2433–7.
186. Rozental TD, Walley KC, Demissie S, Caksa S, Martinez-Betancourt A, Parker AM, et al. Bone material strength index as measured by impact microindentation in postmenopausal women with distal radius and hip fractures. *J Bone Miner Res*. 2018;33(4):621–6.
187. Sosa DD, Eriksen EF. Reduced bone material strength is associated with increased risk and severity of osteoporotic fractures. An impact microindentation study. *Calcif Tissue Int*. 2017;101(1):34–42.
188. Rudäng R, Zoulakis M, Sundh D, Brisby H, Diez-Perez A, Johansson L, et al. Bone material strength is associated with areal BMD but not with prevalent fractures in older women. *Osteoporos Int*. 2016;27(4):1585–92.
189. Popp KL, Caksa S, Martinez-Betancourt A, Yuan A, Tsai J, Yu EW, et al. Cortical bone material strength index and bone microarchitecture in postmenopausal women with atypical femoral fractures. *J Bone Miner Res*. 2019;34(1):75–82.
190. Guerri-Fernandez RC, Nagues X, Quesada Gomez JM, Torres Del Pliego E, Puig L, Garcia-Giralt N, et al. Microindentation for in vivo measurement of bone tissue material properties in atypical femoral fracture patients and controls. *J Bone Miner Res*. 2013;28(1):162–8.
191. Jenkins T, Coultts LV, D'Angelo S, Dunlop DG, Oreffo RO, Cooper C, et al. Site-dependent reference point microindentation complements clinical measures for improved fracture risk assessment at the human femoral neck. *J Bone Miner Res*. 2016;31(1):196–203.
192. Jenkins T, Katsamenis OL, Andriotis OG, Coultts LV, Carter B, Dunlop DG, et al. The inferomedial femoral neck is compromised by age but not disease: fracture toughness and the multifactorial mechanisms comprising reference point microindentation. *J Mech Behav Biomed Mater*. 2017;75:399–412.
193. Milovanovic P, Rakocevic Z, Djonic D, Zivkovic V, Hahn M, Nikolic S, et al. Nano-structural, compositional and micro-architectural signs of cortical bone fragility at the superolateral femoral neck in elderly hip fracture patients vs. healthy aged controls. *Exp Gerontol*. 2014;55:19–28.
194. Karim L, Van Vliet M, Bouxsein ML. Comparison of cyclic and impact-based reference point indentation measurements in human cadaveric tibia. *Bone*. 2018;106:90–5.
195. Granke M, Coulmier A, Uppuganti S, Gaddy JA, Does MD, Nyman JS. Insights into reference point indentation involving human cortical bone: sensitivity to tissue anisotropy and mechanical behavior. *J Mech Behav Biomed Mater*. 2014;37:174–85.
196. Idkaidek A, Jasiuk I. Modeling of Osteoprobe indentation on bone. *J Mech Behav Biomed Mater*. 2019;90:365–73.
197. Abraham AC, Agarwalla A, Yadavalli A, Liu JY, Tang SY. Microstructural and compositional contributions towards the mechanical behavior of aging human bone measured by cyclic and impact reference point indentation. *Bone*. 2016;87:37–43.
198. Krege JB, Aref MW, McNerny E, Wallace JM, Organ JM, Allen MR. Reference point indentation is insufficient for detecting alterations in traditional mechanical properties of bone under common experimental conditions. *Bone*. 2016;87:97–101.
199. McAndrew CM, Agarwalla A, Abraham AC, Feuchtbaum E, Ricci WM, Tang SY. Local bone quality measurements correlates with maximum screw torque at the femoral diaphysis. *Clin Biomech (Bristol, Avon)*. 2018;52:95–9.
200. Beck TJ, Ruff CB, Warden KE, Scott WWJ, Rao GU. Predicting femoral neck strength from bone mineral data. A structural approach. *Investig Radiol*. 1990;25:6–18.
201. Myers ER, Hecker AT, Rooks DS, Hipp JA, Hayes WC. Geometric variables from DXA of the radius predict forearm fracture load in vitro. *Calcif Tissue Int*. 1993;52(3):199–204.
202. Yoshikawa T, Turner CH, Peacock M, Slemenda CW, Weaver CM, Teegarden D, et al. Geometric

- structure of the femoral neck measured using dual-energy x-ray absorptiometry [published erratum appears in *J Bone Miner Res* 1995 Mar;10(3):510]. *J Bone Miner Res*. 1994;9(7):1053–64.
203. Beck TJ, Oreskovic TL, Stone KL, Ruff CB, Ensrud K, Nevitt MC, et al. Structural adaptation to changing skeletal load in the progression toward hip fragility: the study of osteoporotic fractures. *J Bone Miner Res*. 2001;16(6):1108–19.
 204. Beck TJ, Ruff CB, Scott WW Jr, Plato CC, Tobin JD, Quan CA. Sex differences in geometry of the femoral neck with aging: a structural analysis of bone mineral data. *Calcif Tissue Int*. 1992;50:24–9.
 205. Moro M, van der Meulen MCH, Kiratli BJ, Marcus R, Bachrach LK, Carter DR. Body mass is the primary determinant of midfemoral bone acquisition during adolescent growth. *Bone*. 1996;19(5):519–26.
 206. Baker AM, Wagner DW, Kiratli BJ, Beaupre GS. Pixel-based DXA-derived structural properties strongly correlate with pQCT measures at the one-third distal femur site. *Ann Biomed Eng*. 2017;45(5):1247–54.
 207. Villa-Camacho JC, Iyoha-Bello O, Behrouzi S, Snyder BD, Nazarian A. Computed tomography-based rigidity analysis: a review of the approach in preclinical and clinical studies. *Bonekey Rep*. 2014;3:587.
 208. Hong J, Cabe GD, Tedrow JR, Hipp JA, Snyder BD. Failure of trabecular bone with simulated lytic defects can be predicted non-invasively by structural analysis. *J Orthop Res*. 2004;22(3):479–86.
 209. Whealan KM, Kwak SD, Tedrow JR, Inoue K, Snyder BD. Noninvasive imaging predicts failure load of the spine with simulated osteolytic defects. *J Bone Joint Surg Am*. 2000;82(9):1240–51.
 210. Windhagen HJ, Hipp JA, Silva MJ, Lipson SJ, Hayes WC. Predicting failure of thoracic vertebrae with simulated and actual metastatic defects. *Clin Orthop Relat Res*. 1997;344:313–9.
 211. Morgan EF, Keaveny TM. Dependence of yield strain of human trabecular bone on anatomic site. *J Biomech*. 2001;34(5):569–77.
 212. Snyder BD, Hauser-Kara DA, Hipp JA, Zurakowski D, Hecht AC, Gebhardt MC. Predicting fracture through benign skeletal lesions with quantitative computed tomography. *J Bone Joint Surg Am*. 2006;88(1):55–70.
 213. Buckley JM, Loo K, Motherway J. Comparison of quantitative computed tomography-based measures in predicting vertebral compressive strength. *Bone*. 2007;40(3):767–74.
 214. Buckley JM, Cheng L, Loo K, Slyfield C, Xu Z. Quantitative computed tomography-based predictions of vertebral strength in anterior bending. *Spine*. 2007;32(9):1019–27.
 215. Bouxsein ML, Melton LJ 3rd, Riggs BL, Muller J, Atkinson EJ, Oberg AL, et al. Age- and sex-specific differences in the factor of risk for vertebral fracture: a population-based study using QCT. *J Bone Miner Res*. 2006;21(9):1475–82.
 216. Riggs BL, Melton LJ 3rd, Robb RA, Camp JJ, Atkinson EJ, Oberg AL, et al. Population-based analysis of the relationship of whole bone strength indices and fall-related loads to age- and sex-specific patterns of hip and wrist fractures. *J Bone Miner Res*. 2006;21(2):315–23.
 217. Snyder BD, Cordio MA, Nazarian A, Kwak SD, Chang DJ, Entezari V, et al. Noninvasive prediction of fracture risk in patients with metastatic cancer to the spine. *Clin Cancer Res*. 2009;15(24):7676–83.
 218. Leong NL, Anderson ME, Gebhardt MC, Snyder BD. Computed tomography-based structural analysis for predicting fracture risk in children with benign skeletal neoplasms: comparison of specificity with that of plain radiographs. *J Bone Joint Surg Am*. 2010;92(9):1827–33.
 219. Keaveny TM, Donley DW, Hoffmann PF, Mitlak BH, Glass EV, San Martin JA. Effects of teriparatide and alendronate on vertebral strength as assessed by finite element modeling of QCT scans in women with osteoporosis. *J Bone Miner Res*. 2007;22(1):149–57.
 220. Lian KC, Lang TF, Keyak JH, Modin GW, Rehman Q, Do L, et al. Differences in hip quantitative computed tomography (QCT) measurements of bone mineral density and bone strength between glucocorticoid-treated and glucocorticoid-naïve postmenopausal women. *Osteoporos Int*. 2005;16(6):642–50.
 221. Cody DD, Hou FJ, Divine GW, Fyhrie DP. Femoral structure and stiffness in patients with femoral neck fracture. *J Orthop Res*. 2000;18(3):443–8.
 222. Crawford RP, Cann CE, Keaveny TM. Finite element models predict in vitro vertebral body compressive strength better than quantitative computed tomography. *Bone*. 2003;33(4):744–50.
 223. Keyak JH, Kaneko TS, Tehranzadeh J, Skinner HB. Predicting proximal femoral strength using structural engineering models. *Clin Orthop Relat Res*. 2005;437:219–28.
 224. Bessho M, Ohnishi I, Matsuyama J, Matsumoto T, Imai K, Nakamura K. Prediction of strength and strain of the proximal femur by a CT-based finite element method. *J Biomech*. 2007;40(8):1745–53.
 225. Cody DD, Gross GJ, Hou FJ, Spencer HJ, Goldstein SA, Fyhrie DP. Femoral strength is better predicted by finite element models than QCT and DXA. *J Biomech*. 1999;32(10):1013–20.
 226. Dall'Ara E, Luisier B, Schmidt R, Kainberger F, Zysset P, Pahr D. A nonlinear QCT-based finite element model validation study for the human femur tested in two configurations in vitro. *Bone*. 2013;52(1):27–38.
 227. Dall'Ara E, Schmidt R, Pahr D, Varga P, Chevalier Y, Patsch J, et al. A nonlinear finite element model validation study based on a novel experimental technique for inducing anterior wedge-shape fractures in human vertebral bodies in vitro. *J Biomech*. 2010;43(12):2374–80.
 228. Dragomir-Daescu D, Op Den Buijs J, McEligot S, Dai Y, Entwistle RC, Salas C, et al. Robust QCT/

- FEA models of proximal femur stiffness and fracture load during a sideways fall on the hip. *Ann Biomed Eng.* 2011;39(2):742–55.
229. Koivumaki JE, Thevenot J, Pulkkinen P, Kuhn V, Link TM, Eckstein F, et al. Ct-based finite element models can be used to estimate experimentally measured failure loads in the proximal femur. *Bone.* 2012;50(4):824–9.
 230. Liebschner MA, Kopperdahl DL, Rosenberg WS, Keaveny TM. Finite element modeling of the human thoracolumbar spine. *Spine (Phila Pa 1976).* 2003;28(6):559–65.
 231. Nishiyama KK, Gilchrist S, Guy P, Crompton P, Boyd SK. Proximal femur bone strength estimated by a computationally fast finite element analysis in a sideways fall configuration. *J Biomech.* 2013;46(7):1231–6.
 232. Johannesdottir F, Thrall E, Muller J, Keaveny TM, Kopperdahl DL, Bouxsein ML. Comparison of non-invasive assessments of strength of the proximal femur. *Bone.* 2017;105:93–102.
 233. Keyak JH, Sigurdsson S, Karlsdottir G, Oskarsdottir D, Sigmarsdottir A, Zhao S, et al. Male-female differences in the association between incident hip fracture and proximal femoral strength: a finite element analysis study. *Bone.* 2011;48(6):1239–45.
 234. Keyak JH, Sigurdsson S, Karlsdottir GS, Oskarsdottir D, Sigmarsdottir A, Kornak J, et al. Effect of finite element model loading condition on fracture risk assessment in men and women: the AGES-Reykjavik study. *Bone.* 2013;57(1):18–29.
 235. Lang TF, Sigurdsson S, Karlsdottir G, Oskarsdottir D, Sigmarsdottir A, Chengshi J, et al. Age-related loss of proximal femoral strength in elderly men and women: the Age Gene/Environment Susceptibility Study--Reykjavik. *Bone.* 2012;50(3):743–8.
 236. Eberle S, Gottlinger M, Augat P. An investigation to determine if a single validated density-elasticity relationship can be used for subject specific finite element analyses of human long bones. *Med Eng Phys.* 2013;35(7):875–83.
 237. Schileo E, Dall'ara E, Taddei F, Malandrino A, Schotkamp T, Baleani M, et al. An accurate estimation of bone density improves the accuracy of subject-specific finite element models. *J Biomech.* 2008;41(11):2483–91.
 238. Eberle S, Gottlinger M, Augat P. Individual density-elasticity relationships improve accuracy of subject-specific finite element models of human femurs. *J Biomech.* 2013;46(13):2152–7.
 239. Enns-Bray WS, Bahaloo H, Fleps I, Ariza O, Gilchrist S, Widmer R, et al. Material mapping strategy to improve the predicted response of the proximal femur to a sideways fall impact. *J Mech Behav Biomed Mater.* 2018;78:196–205.
 240. Zysset PK, Dall'ara E, Varga P, Pahr DH. Finite element analysis for prediction of bone strength. *Bonekey Rep.* 2013;2:386.
 241. van Rietbergen B, Ito K. A survey of micro-finite element analysis for clinical assessment of bone strength: the first decade. *J Biomech.* 2015;48(5):832–41.
 242. Boutroy S, Van Rietbergen B, Sornay-Rendu E, Munoz F, Bouxsein ML, Delmas PD. Finite element analysis based on in vivo HR-pQCT images of the distal radius is associated with wrist fracture in postmenopausal women. *J Bone Miner Res.* 2008;23(3):392–9.
 243. Liu XS, Zhang XH, Sekhon KK, Adams MF, McMahon DJ, Bilezikian JP, et al. High-resolution peripheral quantitative computed tomography can assess microstructural and mechanical properties of human distal tibial bone. *J Bone Miner Res.* 2010;25(4):746–56.
 244. MacNeil JA, Boyd SK. Accuracy of high-resolution peripheral quantitative computed tomography for measurement of bone quality. *Med Eng Phys.* 2007;29(10):1096–105.
 245. Varga P, Zysset PK. Assessment of volume fraction and fabric in the distal radius using HR-pQCT. *Bone.* 2009;45(5):909–17.
 246. Macneil JA, Boyd SK. Bone strength at the distal radius can be estimated from high-resolution peripheral quantitative computed tomography and the finite element method. *Bone.* 2008;42(6):1203–13.
 247. Mueller TL, Christen D, Sandercott S, Boyd SK, van Rietbergen B, Eckstein F, et al. Computational finite element bone mechanics accurately predicts mechanical competence in the human radius of an elderly population. *Bone.* 2011;48(6):1232–8.
 248. Pistoia W, van Rietbergen B, Lochmuller EM, Lill CA, Eckstein F, Ruegsegger P. Image-based micro-finite-element modeling for improved distal radius strength diagnosis: moving from bench to bedside. *J Clin Densitom.* 2004;7(2):153–60.
 249. Varga P, Pahr DH, Baumbach S, Zysset PK. HR-pQCT based FE analysis of the most distal radius section provides an improved prediction of Colles' fracture load in vitro. *Bone.* 2010;47(5):982–8.
 250. Zhou B, Wang J, Yu YE, Zhang Z, Nawathe S, Nishiyama KK, et al. High-resolution peripheral quantitative computed tomography (HR-pQCT) can assess microstructural and biomechanical properties of both human distal radius and tibia: ex vivo computational and experimental validations. *Bone.* 2016;86:58–67.
 251. Vilayphiou N, Boutroy S, Sornay-Rendu E, Van Rietbergen B, Munoz F, Delmas PD, et al. Finite element analysis performed on radius and tibia HR-pQCT images and fragility fractures at all sites in postmenopausal women. *Bone.* 2010;46(4):1030–7.
 252. Vilayphiou N, Boutroy S, Szulc P, van Rietbergen B, Munoz F, Delmas PD, et al. Finite element analysis performed on radius and tibia HR-pQCT images and fragility fractures at all sites in men. *J Bone Miner Res.* 2011;26(5):965–73.
 253. Kroker A, Plett R, Nishiyama KK, McErlain DD, Sandino C, Boyd SK. Distal skeletal tibia assessed by HR-pQCT is highly correlated with femoral and lumbar vertebra failure loads. *J Biomech.* 2017;59:43–9.